1	Microbial community biomass, production and grazing along 110°E
2	in the eastern Indian Ocean
3	
4	Michael R. Landry <sup>a*</sup> , Raleigh R. Hood <sup>b</sup> , Claire H. Davies <sup>c</sup> , Karen E. Selph <sup>d</sup> , David Antoine <sup>e,f</sup> ,
5	Mika C. Carla, Lynnath E. Beckleyg
6	
7	<sup>a</sup> Scripps Institution of Oceanography, University of California at San Diego, La Jolla, CA
8	92093-0227, USA
9	<sup>b</sup> Horn Point Laboratory, University of Maryland Center for Environmental Science, Cambridge
10	MD, USA
11	<sup>c</sup> CSIRO Oceans and Atmosphere, Castray Esplanade, Hobart, Tasmania 7000 Australia
12	<sup>d</sup> Department of Oceanography, University of Hawai'i at Manoa, Honolulu, HI 96822, USA
13	<sup>e</sup> Remote Sensing and Satellite Research Group, School of Earth and Planetary Sciences, Curtin
14	University, Perth, WA 6845, Australia
15	<sup>f</sup> Sorbonne Université, CNRS, Laboratoire d'Océanographie de Villefranche, LOV, F-06230
16	Villefranche-sur-Mer, France
17	<sup>g</sup> Environmental and Conservation Sciences, Murdoch University, Murdoch 6150, Western
18	Australia
19	
20	
21	*Corresponding author
22	E-mail address: mlandry@ucsd.edu (M.R. Landry)
23	
24	Keywords: phytoplankton growth, production, microzooplankton grazing, picoplankton,
25	Prochlorococcus, heterotrophic bacteria, subtropical, tropical
26	

# ABSTRACT

27

28 We investigated plankton biomass structure, production and grazing rates from temperate to 29 tropical waters (39.5-11.5°S) along the historic 110°E transect in the eastern Indian Ocean 30 (IO) during May-June 2019. The timing captures the seasonal transition from moderate 31 productivity in the subtropical sector to seasonally high primary production in tropical waters 32 as described in IIOE (International Indian Ocean Expedition) studies of the 1960s. Carbon-33 based estimates of phytoplankton production and microzooplankton grazing were determined 34 from depth profiles of dilution incubations analyzed by flow cytometry and pigments; 35 mesozooplankton biomass and grazing were determined from net sampling and gut 36 fluorescence for the integrated euphotic zone. Phytoplankton biomass varied from 860 to 1740 mg C m<sup>-2</sup>, averaging 1187 mg C m<sup>-2</sup> with no latitudinal trend. Mixed-layer C:Chla 37 38 ranged from 20-40 in the nitrogen-rich subtropical front to 100-180 in tropical waters. 39 Prochlorococcus increased from 141 to 915 mg C m<sup>-2</sup> between 39.5°S and 20°S and averaged 40 700 mg C m<sup>-2</sup> at lower latitudes. Synechococcus and photosynthetic eukaryotes contributed least to biomass (3.6 and 30.5%, respectively) at mid-transect locations (15.5-27.5°S). 41 42 Dinoflagellates and diatoms were typically rare (28 and 6 mg C m<sup>-2</sup>, respectively). Among heterotrophs, bacteria averaged 476 mg C m<sup>-2</sup>, with a subtropical front maximum but no 43 latitudinal trend; ciliates averaged 112 mg C m<sup>-2</sup>, and mesozooplankton increased 44 significantly south-to-north (131-488 mg C m<sup>-2</sup>). Phytoplankton production and grazing 45 46 averaged 466 and 461 mg C m<sup>-2</sup> d<sup>-1</sup>, respectively, based on the sums for flow-cytometry 47 measured populations, and 618 and 604 mg C m<sup>-2</sup> d<sup>-1</sup>, respectively, based on Chla-determined 48 rates. Our results highlight key relationships that link stocks and process rates across 49 oceanographic provinces of the eastern IO. Production and grazing increased 6-8 fold from 50 south to north. *Prochlorococcus* dominated productivity, and microzooplankton accounted 51 for 85-89% of grazing. Production and grazing were strongly coupled and balanced on 52 average. Over the transect, increasing growth conditions (light and temperature) mainly 53 manifested as more rapid biomass turnover and mesozooplankton biomass accumulation. 54

#### 1. Introduction

55

56

57

58

59

60

61

62

63

64

65

66

67

68

69

70

71

72

73

74

75

76

77

78

79

80

81

82

83

84

85

Low-latitude waters of the Indian Ocean (IO) absorb most of the excess heat from the Pacific Ocean that flows through the Indonesian Throughflow (ITF) and have been warming faster than comparable areas of the Atlantic and Pacific (Lee et al., 2015; Desbruyéres et al., 2017), with satellite observations also suggesting the largest decline of phytoplankton biomass (Gregg and Rousseaux, 2019). Yet the IO remains the most sparsely studied ocean, with precious little data for evaluating long-term changes in ecosystem structure and function. The last major systemlevel investigation of the southeastern IO was the International Indian Ocean Expedition (IIOE) of the 1960's. From bimonthly cruises conducted along longitude 110°E from August 1962 to August 1963, Australian oceanographers of that era did a remarkable job describing the complexities of regional circulation and forcing (Rochford, 1969, 1977), the distributions of nutrients, phytoplankton chlorophyll and particulate carbon (Humphrey and Kerr, 1969; Newell, 1969; Rochford, 1963), and the seasonal cycles of primary production and mesozooplankton (Jitts 1969; Tranter and Kerr, 1969, 1977), with an emphasis on diverse zooplankton groups and species (McWilliam, 1977; Sakthivel, 1977; Tranter, 1977a,b). Nonetheless, this early effort preceded many key discoveries that constitute the modern foundation of pelagic food web understanding: the revolutionary paradigm of the microbial loop (Azam et al, 1983), ubiquitous and abundant photosynthetic bacteria (Waterbury et al., 1979; Chisholm et al., 1988), dominant grazing roles of protistan microzooplankton (Calbet and Landry, 2004), and even the methodology to make systematic measurements of zooplankton grazing of any kind. While some of these missing food-web components have been considered in the few regional studies since IIOE, those have tended to focus on comparative investigations of distinct mesoscale features and their implications for fisheries recruitment (Waite et al., 2007b, 2019; Wang et al., 2014; Säwström et al., 2014) as well as latitudinal and mesoscale variability along the Leeuwin Current (e.g., Thompson et al., 2012; Lourey et al., 2013; Sutton and Beckley, 2016). Thus, it remains difficult to assess possible decadal changes due to anthropogenic climate impacts or to place the contemporary dynamics of the eastern IO in the context of other well-studied ecosystems. R/V Investigator cruise IN2019 V03 was undertaken as part of IIOE-2 (Second International Indian Ocean Expedition) to improve understanding of physical, biogeochemical and trophic

processes across temperate to tropical oceanic waters of the historic 110°E transect, with the goal

86 of providing a modern perspective to facilitate development of regional physical-biogeochemical 87 models (Beckley et al., this volume). As part of this expedition, we conducted sampling and 88 experiments to compare biomass, production and grazing from bacteria to mesozooplankton at 89 20 stations from 39.5 to 11.5°S. Our study, comprising the first integrated investigation of 90 plankton community structure and food-web dynamics in the eastern IO, was motivated by 91 several basic questions: What are the key relationships that link stocks and process rates across 92 different oceanographic provinces over this broad latitudinal extent? How do they relate to 93 previous IIOE descriptions along 110°E, and, where comparisons can be made, are there 94 indications of significant change over the intervening six decades? How do the measurements 95 and relationships relate to findings from similarly conducted investigations in other tropical and 96 subtropical ecosystems?

## 2. Materials and methods

97

98

#### 2.1. Sampling and experimental set-up

99 Sampling and experiments were conducted at 20 stations on the 110°E transect from 17 May 100 to 5 June 2019 on R/V Investigator cruise IN2019 V03 (Fig. 1a, Table 1). The stations, spaced mostly 1.5° apart from 39.5 to 11.5°S, were occupied on successive days according to a 101 102 consistent daily schedule, followed by late-night transit between stations. Mean light extinction 103 coefficients for the euphotic zone were determined from PAR (Photosynthetically Active 104 Radiation) profiles in morning (~10:00) CTD hydrocasts. Mesozooplankton net tows were taken 105 at mid-day (~13:30) and 1-2 hours after local sunset (~19:30) with a 1-m diameter ring net (0.2-106 mm Nitex mesh, General Oceanics flowmeter and Senus Ultra time-depth-temperature recorder) 107 towed obliquely through the euphotic zone at a ship speed of 1.5 kt (Landry et al., 2020a). 108 Seawater for microplankton community analyses and to set-up dilution experiments was 109 collected on evening CTD hydrocasts (~21:00) at light depths determined from the morning cast 110 of 76, 32, 18, 7.6, 2.6 and 1.3% of incident PAR, hereafter %I<sub>o</sub>, corresponding to the 111 transmission characteristics of six incubator containers described below. Seawater samples (2.3 112 L) for pigment analyses by high pressure liquid chromatography (HPLC) were also collected on 113 the same evening CTD hydrocasts as samples for microplankton community analyses, but in 114 different bottles and generally at different depths, following a semi-fixed depth plan (e.g., 5, 10, 115 25, 50, 75, 100 m, etc.). To compare HPLC results from fixed depths to samples collected at

light depths, we interpolated measurements from the fixed depths to values at the sampled light depths.

For each light-depth sampled, we prepared a two-treatment dilution experiment (Landry et al., 2008, 2011), with one polycarbonate bottle (2.7 L) containing unfiltered seawater (100%) and the second (diluted) bottle consisting of ~33% whole seawater with filtered water from the same depth. Seawater was filtered directly from the Niskin bottles using a peristaltic pump, silicone tubing and an in-line 0.2-µm Suporcap filter capsule that had previously been acid washed. Dilution bottles were first given a measured volume of filtered water and then gently filled to the top with unscreened water from the Niskin bottles to avoid physical damage to fragile protists (Gifford, 1988; Lessard and Murrell, 1998), and no nutrients were added. Lessard and Murrell (1998) demonstrated that added nutrients were not needed for rate linearity in oligotrophic systems, while added nutrients often resulting in erratic results and depressed grazing. After preparation, each bottle was subsampled for flow cytometric (FCM, 2 mL) analyses of initial concentrations and volumetric dilution factors. The paired bottles from each depth were placed in their respective incubator boxes for 24 h, cooled with constant high flow from the ship's running seawater line. The incubators were covered to protect from deck lighting during nighttime operations and received full solar lighting during the daytime.

Each incubator was constructed with an outer box and lid of clear, light blue (#2069) or dark blue (#2424) Plexiglas and inner panels and lids of neutral density acrylic. Samples of each component were analyzed separately with a Cary 300 spectrophotometer for spectral transmission from 375 to 750 nm, and the outer box colors and inner filters were matched to mimic the reduced transmission and blue spectral shift with depth. After construction, each incubator was calibrated for exact % transmission with a  $4\pi$  PAR sensor inside the water-filled incubators relative to simultaneous measurements of incident PAR with a  $2\pi$  sensor.

#### 2.2. Environmental measurements

Temperature and salinity were measured during sample collection by CTD sensors and direct shipboard analyses (Guildline 8400B salinometer). Incubation temperature is the mean of two sensors in the ship's running seawater line, recorded at 5-min intervals and daily averaged. Daily incident solar light (PAR, moles photon flux m<sup>-2</sup> d<sup>-1</sup> = E m<sup>-2</sup> d<sup>-1</sup>) is the mean of two Licor LI-190 PAR sensors positioned on the ship's port and starboard sides, integrated over the

photoperiod from measured µE m<sup>-2</sup> s<sup>-1</sup> at 5-min intervals. Wind speed was also measured by two 146 147 instruments (RM Young 05106 Propellor anemometer, Gill WindObserver II Ultrasonic 148 anemometer) and averaged for the daytime as an indicator of day-to-day variability in wind 149 mixing energy. Nutrients were analyzed on board by the CSIRO hydrochemistry group using a 150 Seal AA3HR segmented-flow autoanalyzer (Rees et al., 2018). Analyses were standardized to 151 certified reference material and had detection limits of 0.02 µM for nitrate+nitrite and phosphate, 152 0.2 µM for silicate, and 0.01 µM for ammonium. 153 2.3. Flow cytometric analyses 154 Picophytoplankton FCM samples were preserved with 3% paraformaldehyde and frozen at – 80°C. Thawed samples were stained with Hoechst 34580 (1 μg mL<sup>-1</sup>; Monger and Landry, 155 156 1993) and analyzed at a flow rate of 30 µL min<sup>-1</sup> with a Beckman-Coulter CytoFLEX-S 157 cytometer with 4 lasers (Selph, 2021b). Side scatter, forward angle light scatter (FALS) and 158 fluorescence signals were measured using laser excitation (EX)/emission (EM) filters of 159 EX375/EM450±45 for Hoechst-stained DNA, EX488/EM690±50 for chlorophyll, and 160 EX561/EM585±42 for phycoerythrin. Listmode files (FCS 3.0) were analyzed with FlowJo 161 software (v.10.6.1) for abundances of *Prochlorococcus* (PRO), *Synechococcus* (SYN), 162 photosynthetic eukaryotes (EUK) and heterotrophic bacteria (HBAC), as well as their 163 population-average fluorescence and scatter signals normalized to fluorescent microbead 164 standards. 165 Population carbon estimates were determined from cell abundances and mean cell carbon 166 scaled to relative cell sizes. For PRO, we assumed a base value of 32 fg C cell-1 (Garrison et al., 167 2000) and a mean diameter of 0.65 µm for subtropical surface waters. Base values for SYN and EUK were scaled proportionally to 155 and 3150 fg C cell<sup>-1</sup> for cells of 1.1 and 3.0 μm 168 169 diameters, respectively. For HBAC, we used a base value of 11 fg C cell-1 (Garrison et al., 170 2000). To account for cell carbon variability due to cell size differences along the transect and with depth, we used the bead-normalized FALS ratio (FALS<sub>i</sub>/FALS<sub>b</sub>)<sup>0.55</sup> as a measure of the 171 172 relative cell biovolume in sample i compared to the base value b (Landry et al., 2003), which 173 comes from the near-linear relationship between FALS and Mie scattering cross section for cells 174 in the submicron-micron size range (DuRand and Olson, 1996). For chlorophyll-containing

175 populations, mean bead-normalized red fluorescence captured by filter EM690±50 was used as a 176 relative measure of cell Chla content. 177 2.4. Pigment and microscopical analyses 178 Initial and final samples (500 mL) for shipboard fluorometric Chla analyses of dilution 179 experiments were filtered onto GF/F filters and extracted with 90% acetone in a -20°C freezer 180 for 24 h. Extracted samples were warmed to room temperature in the dark and analyzed on a 181 Turner Designs model 10 fluorometer calibrated against a pure Chla standard (Strickland and 182 Parsons, 1972). 183 Samples (2.3 L) for analyses of chlorophyll and carotenoid pigments by high-pressure liquid 184 chromatography (HPLC) were concentrated onto Whatman GF/F filters under low vacuum 185 pressure, immediately frozen in liquid nitrogen, and stored at -80°C. The samples were extracted 186 for 2 h in 100% methanol, disrupted by sonication, clarified by GF/F filtration and analyzed by 187 HPLC (Agilent Technologies 1200 Series) at the analytical facility of the Institut de la Mer de 188 Villefranche (CNRS-France) according to procedures described in Ras et al. (2008). 189 Seawater samples (250 mL) were also preserved with 5% acid Lugol's solution for 190 microscopical analyses of select protists by the Utermöhl method (Lund et al., 1958). For the 191 present analysis, samples from the upper three sampling depths (76, 33 and 18% I<sub>0</sub>) were 192 volumetrically combined to produce one sample representing the upper euphotic zone. Over a 193 process taking several days, the combined sample was measured for total volume in a volumetric 194 cylinder, settled for 24 h, concentrated by suctioning off the upper water and ultimately settled 195 and analyzed in an Utermöhl chamber. All recognizable ciliates, dinoflagellates and diatoms on 196 the resulting slide were imaged on a Zeiss AxioVert 200 M inverted microscope at 200X 197 magnification using brightfield illumination and processed using Image Pro software. For 198 ciliates, we calculated carbon biomass as pg  $C = 0.19 \times BV$  (Putt and Stoecker, 1989) based on 199 cell biovolumes (BV, um<sup>3</sup>) from length and width measurements and the most appropriate cell 200 shapes. For dinoflagellates and diatoms, C biomass was computed from the equations of

Menden-Deuer and Lessard (2000). Measured biomass concentrations for the upper EZ were

extrapolated to the depth of the full EZ assuming uniform mixing.

201

202

## 2.3. Microbial growth and grazing rates

We determined rate profiles for phytoplankton growth (μ, d<sup>-1</sup>) and microzooplankton grazing (m, d<sup>-1</sup>) from each pair of dilution experiment bottles and for each FCM population and Chl*a* according to the following equations:

208 
$$m = (k_d - k)/(1 - D)$$
 and  $\mu = k + m$ ,

where  $k_d$  and k are the measured net rates of change between initial and final concentrations in the diluted and undiluted treatments, respectively, and D (= 0.33) is the portion of unfiltered water in the dilution treatment (Landry et al., 2008; Selph et al., 2011). Rate estimates assume comparable growth rates in dilution treatments and proportional grazing relative to dilution, consistent with the expected close coupling of production, grazing and nutrient remineralization in microbial communities of oligotrophic systems. Rate estimates for FCM populations are from cell abundances. Chla-based rates are from fluorometer readings and mean acid ratios from initial and final treatments at each experimental depth, with growth rates corrected for change in cell Chla:C content, determined as Ln [(RF:C)<sub>final</sub> / (RF:C)<sub>init</sub>], where RF and C are community totals for bead-normalized red fluorescence and carbon, respectively. Carbon-based estimates of phytoplankton production (PROD) and microzooplankton grazing (MICRO GRAZ) were calculated from growth ( $\mu$ ) and grazing (m) rates for total Chla from dilution experiments and the following equations (Landry et al., 2000):

PROD = 
$$\mu \times C_o (e^{(\mu-m)t} - 1)/(\mu - m)t$$
, and

223 
$$MICRO GRAZ = m \times C_o (e^{(\mu-m)t} - 1)/(\mu - m)t$$

- where  $C_0$  is initial autotrophic biomass (mg C m<sup>-3</sup>) and t = time (1 day). PROD and MICRO
- GRAZ estimates for the euphotic zone were determined by integrating individual rate estimates
- from the surface to the deepest incubation depth according to the trapezoidal rule.

## 227 2.4 Mesozooplankton biomass and grazing

Details of mesozooplankton biomass and grazing along 110°E are presented in Landry et al. (2020a). Briefly, the net tow samples were anesthetized with CO<sub>2</sub> (ice-cold soda water) and a sea-ice ice slurry (-1.8°C), split into two ¼ sample fractions with a Folsom plankton splitter, and separately wet sieved through Nitex screens to produce two sets of 5 size classes: 0.2-0.5, 0.5-1, 1-2, 2-5 and >5 mm (the remaining ½ sample was formaldehyde preserved). One size-fractioned set was oven dried on pre-weighed Nitex filters, reweighed for dry weight (DW), then ground to

a powder and subsampled for analyses of C:DW and N:DW contents on a Perkin Elmer CHN analyzer. Mesozooplankton biomass (C m<sup>-2</sup>) was calculated from the sum of size-fractioned samples, the tow depths and the tow distances assuming 100% net capture efficiency. We averaged day and night tows for station mean biomass.

The second size-fraction set was analyzed on shipboard by the gut fluorescence method (Mackas and Bohrer, 1976). Samples were homogenized with 7 mL of 90% acetone in an ice bath with a Vibracell sonicator probe, extracted overnight at -20°C and warmed to room temperature prior to analysis. The homogenate was shaken and centrifuged to remove particulates, and Chla and phaeopigment (Phaeo) concentrations were measured by the acidification method using a 10AU fluorometer (Strickland and Parsons, 1972). We estimated grazing rates (G, mg pigment m-2 time-1) as G = GPC \* K, where GPC is the gut Phaeo content and K (min-1) = 0.0026 (T°C) + 0.012 is the gut evacuation rate constant from Irigoien (1998). Mesozooplankton grazing impact on the phytoplankton community m-2 was calculated from the percent of water-column Chla consumed d-1 integrated to the tow depth and averaged for day and night tows. C-based grazing estimates (MESO GRAZ below) were computed from EZ-integrated mean estimates of phytoplankton C:Chla.

#### 3. Results

238

239

240

241

242

243

244

245

246

247

248

249

250

251

262

263

#### 3.1. Environmental conditions

- 252 Temperature and salinity define two major water masses along the 110°E transect (Fig. 1b,c).
- 253 The high-salinity surface water (>35.7 psu) between ~27.5 and 35°S is a distinctive feature of the
- southern IO subtropical region that sinks below lower density water to the north (Rochford,
- 255 1969; Woo and Pattiaratchi, 2008). We refer to this as subtropical water (STW; Wyrtki, 1973).
- 256 The high-temperature, low-salinity water mass north of 14°S enters the Indian Ocean from the
- 257 Pacific via the ITF and is referred to here as Indonesian Throughflow Water (ITW; Talley,
- 258 1995). Between STW and ITW is a zone (15.5-26°S) of high eddy activity and mixing with
- 259 intermediate T-S properties and a subsurface salinity maximum between 150 and 250 m. South
- of the STW (>36°S) is the subtropical front where colder, lower-salinity subantarctic water
- 261 converges with and subducts under the subtropical water mass.
  - Nitrate+nitrite and fluorescence sections show a generally positive relationship over the transect (Fig. 1d,e). Fluorescence is highest, 0.5-0.6 mg Chla m<sup>-3</sup>, in surface water of the

subtropical front where nitrate+nitrite concentrations are elevated. Deep Chlorophyll Maxima (DCM) are mainly evident in the northern half of the transect where significant concentrations of nitrate+nitrite penetrate into the upper 100 m. The DCM is very faint or absent in the STW region, where mixed-layer depth (MLD, Fig. 1d) is deepest along the transect, though not intersecting the nitracline, as it does in the ITW region. MLD shallows to <50 m though most of the mixing region between STW and ITW (Fig. 1d).

The euphotic zone (EZ), here defined by the depth of penetration of 1% incident PAR, varied from 66 to 108 m and averaged  $86 \pm 12$  m for the transect (Fig. 1e). Temperature profiles for the light depths sampled for community analyses and experimental incubations show relatively well-mixed conditions for the EZs overall, but the deeper sampling depths (1.5-2.5 %  $I_o$ ) enter the upper thermocline at some stations in the northern half of the transect (Fig. 2a). This is especially evident in the nitrate+nitrite profiles at 11.5, 12.5, 18.5 and 21.5°S (Fig. 2b), which show substantial concentrations of 1-8  $\mu$ M in the lower EZ. Except for stations in the subtropical front (36.5-39.5°S), nitrate+nitrite concentrations are extremely low (mean  $\pm$  SEM, 0.024  $\pm$  0.002  $\mu$ M) at most stations down to the 7.6 %  $I_o$  light depth (Landry et al., 2022). Conversely, silicate (not shown) was most depleted (0.4-0.7  $\mu$ M) throughout the EZ at the subtropical front stations, while upper EZ concentrations generally exceeded 2  $\mu$ M at all stations north of 32°S (range 1.7-2.7  $\mu$ M; Landry et al., 2022). Phosphate concentrations exceeded nitrate+nitrite in the upper EZ at all stations north of 35°S (range 0.03-0.07  $\mu$ M; Landry et al., 2022).

Although the ranges are similar (0.06-0.60 mg Chla m<sup>-3</sup>), the extracted Chla concentrations from small discrete samples are more variable than suggested by the smooth CTD fluorescence profiles (Fig. 2c). For all but two stations (14 and 38°S), surface concentrations are <0.4 mg Chla m<sup>-3</sup>.

The environmental conditions experienced by the microbial community during incubation experiments differ in some ways from the conditions in the ambient water column. Consistent with the deeply mixed thermal structure, daily-averaged wind speeds were relatively strong, averaging  $27 \pm 2$  km h<sup>-1</sup> for the transect (range 12-45 km h<sup>-1</sup>; Table 1). The freely mixed communities in the water column on the day preceding sampling experienced the strong south-to-north conditions of increasing temperature (Fig. 2a) and incident PAR, ranging from 5 to 37 E m<sup>-2</sup> d<sup>-1</sup> (Table 1). Bottle-contained communities in the experiments were in incubator boxes at

- constant relative percentages of incident PAR and also, due to transits between stations, experienced the sea surface temperature and PAR at 1.5° lower latitude stations during the following day. The differences between ambient and experimental temperatures vary from 0 to  $2.8^{\circ}$ C, averaging  $+0.84 \pm 0.15^{\circ}$ C, with larger differences at the southern end of the transect with the strongest latitudinal gradient in temperature. For PAR, significant (1.5X) differences between prior ambient light history and experimental conditions are mainly seen at scattered stations, with substantially higher incubation PAR at 36.5 and 27.5 °S and substantially lower incubation PAR at 38 and 11.5 °S (Table 1).
  - 3.2. Chlorophyll and carbon biomass relationships

- Population red fluorescence from FCM (cell abundance x mean RF cell<sup>-1</sup>) is strongly correlated to Chla concentrations from the HPLC pigment analyses (Fig. 3). For PRO, RF is related to divinyl Chla (DVChla) by the equation: RF L<sup>-1</sup> =  $10^6 * (0.026 + 2.43 * DVChla L^{-1})$  with R<sup>2</sup> = 0.56, p<10<sup>-6</sup>. For the combined populations of PRO, SYN and EUK, RF L<sup>-1</sup> =  $10^6 * (-0.011 + 3.11 * TChla L^{-1})$  with R<sup>2</sup> = 0.72, p<10<sup>-6</sup>. While slopes of the two relationships have overlapping 95% confidence limits, they do differ significantly (p<0.007), suggesting that the different populations are not identical in cellular RF properties.
  - We applied the mean (±SEM) value from 120 paired comparisons of PRO red fluorescence to DVChla (1 unit RF = 0.432 ± 0.011 fg Chla) to all FCM populations to estimate their respective contributions to EZ-integrated Chla at each station (Fig. 4a,b). Integrated Chla in PRO increases through the subtropical front and STW (39.5 to 29°S) from ~7 to 50% of the total, remains a fairly constant 50-60% of the total through the mixing region, and declines in ITW at stations (12.5-14°S), where SYN increases. SYN Chla is notably higher in the subtropical front and ITW areas and lowest in the mixing region. EUK accounts for the majority of Chla at stations south of 32°S and a relatively consistent ~40% of Chla through the central and northern transect.
  - In comparing the values of integrated Chla from FCM red fluorescence to the station estimates from HPLC (TChl) and fluorometric (FlChl) measurements (Fig. 4c), we observe that RF estimates are closest to FlChl at the southern (32-39.5°S) and northern (11.5-14°S) ends of the transect, while RF corresponds better to TChl for the middle stations. Reasons for these differences are considered in Discussion section 4.1. Here, we note only that in the absence of

clear offsets between RF-based estimates and measured Chla for the transect as a whole, the FCM-measured populations appear to provide a reasonable representation of the total

327 phytoplankton community.

Carbon biomass profiles based on FCM population abundances and FALS-ratio sizing are presented by station in Figure 5. PRO biomass ranges from ~2-12 μg C L<sup>-1</sup> over the transect, increasing generally from south to north (Fig. 5a). SYN biomass exceeds 2 μg C L<sup>-1</sup> only at the southern and northern ends of the transect; biomass declines progressively to minimum levels of 0.3-0.6 μg C L<sup>-1</sup> in the STW and mixing regions and rises to the highest levels 3-4.8 μg C L<sup>-1</sup> at ITW stations 12.5-14°S (Fig. 5b). EUK and HBAC both have their highest biomass values (16-20 and ~9 μg C L<sup>-1</sup>, respectively) in the subtropical front (38-39.5°S) (Fig. 5c,d). EUK biomass declines to 3-5 μg C L<sup>-1</sup> through the STW and mixing regions and is only high again in the ITW at 14°S. (Fig. 5c). HBAC biomass ranges narrowly from 5-7 μg C L<sup>-1</sup> throughout the STW, ITW and mixing regions. EUK is the only FCM-distinguished group with clear and significant deep maxima in C biomass, occurring at the same locations where the upper nitracline intrudes into the base of the euphotic zone (11.5, 12.5, 18.5, 21.5 and 23°S; Figs. 2b,e and 5c).

C:Chla ratios for the individual and combined FCM populations show roughly similar patterns but some variability in ranges (Fig. 6). Near-surface samples for all populations have minimum C:Chla ratios,  $\sim$ 20-40 µg C (µg Chla)<sup>-1</sup>, in the nitrogen-rich subtropical front and highest ratios, 100 to 180 µg C (µg Chla)<sup>-1</sup>, at 11.5 or 14-18.5°S. The range of variability narrows in the deep EZ, approaching the minimum surface values observed at the subtropical front (Fig. 6).

#### 3.3. Integrated carbon biomass for the euphotic zone

In absolute terms, EZ-integrated biomass of PRO increases more-or-less linearly by 6.5 fold from 141 mg C m<sup>-2</sup> at 39.5°S to 915 mg C m<sup>-2</sup> at 20°S, and thereafter averages 700 mg C m<sup>-2</sup> at lower latitudes (Fig. 7a). However, high percent contributions of PRO to phytoplankton C biomass (66.1  $\pm$  2.1%, n=9) occur throughout the broader mixing region (15.5-27.7 °S) between STW and ITW (Fig. 7b). Opposite to the latitudinal trends for PRO, both SYN and EUK have higher integrated C biomass and % contributions in the southern and northern ends of the transect and make their lowest contributions to community C biomass (3.6  $\pm$  0.5 and 30.5  $\pm$  1.8%, respectively) in the region between 15.5-27.7 °S. Despite these substantial shifts in

phytoplankton biomass contributions along the  $110^{\circ}$ E transect, total integrated C varies only by a factor of two (860 to 1740 mg C m<sup>-2</sup>; Fig. 7a). Seventeen of 20 stations exceed 1000 mg C m<sup>-2</sup>, and the transect average is  $1187 \pm 50$  mg C m<sup>-2</sup>.

Consistent with the low variability in HBAC biomass profiles (Fig. 5d), integrated estimates of HBAC biomass are relatively uniform over the transect (Fig. 8a). Aside from the highest value of 616 mg C m<sup>-2</sup> at 39.5°S, all other stations fall within 391 to 542 mg C m<sup>-2</sup>, giving a transect average of  $476 \pm 11$  mg C m<sup>-2</sup>. In contrast, C biomass of mesozooplankton (MESO) exhibits a strong latitudinal trend, with lowest values (131-133 mg C m<sup>-2</sup>) in the south at 32°S and 35-38°S and highest values (426-488 mg C m<sup>-2</sup>) in the ITW at 11.5-14°S (Fig. 8c). Within the ITW region, MESO biomass parallels station variability in total phytoplankton biomass, averaging  $29 \pm 1\%$  of the phytoplankton total. The MESO:PHYTO biomass relationship is lower on average ( $22 \pm 2\%$ ) and more variable (11-37%) for the remaining 17 stations.

The EZ-extrapolated biomass estimates for ciliates and dinoflagellates from microscopical analyses (Fig. 8b) provide a crude approximation of the biomass of larger (>5  $\mu$ m) protists that contribute to grazing, assuming that all dinoflagellates are functionally mixotrophic. The combined sample analyzed for 27.5°S had an anomalously high biomass of *Tripos* spp. that was unlikely to be representative of the EZ as a whole but clearly indicates the potential for enhanced concentrations at small scales. Excluding only the *Tripos* spp. at this station, integrated C biomass for dinoflagellates ranges from 5 to 61 mg C m<sup>-2</sup> and averages  $28 \pm 3$  mg C m<sup>-2</sup> for the transect. Diatoms (not shown) analyzed in the same samples ranged from 0.4 to 35 mg C m<sup>-2</sup> and averaged  $6 \pm 2$  mg C m<sup>-2</sup>. Diatoms and dinoflagellates containing Chl*a* would also have been counted in the photosynthetic EUK category, so they are not in addition to the previously estimated phytoplankton total from the FCM analyses (Fig. 7). Even so, they together comprise <3% of the total biomass estimates, on average, and 6.6% of EUK biomass; thus, these large phytoplankters are a small fraction of the community overall.

Ciliate biomass ranges from 9 to 354 mg C m<sup>-2</sup> and averages  $112 \pm 18$  mg C m<sup>-2</sup> for the transect. Excluding the anomalous *Tripos* spp. biomass at  $27.5^{\circ}$ S, ciliates account for the majority of biomass associated with larger protistan grazers at 19 of the 20 stations, and  $75 \pm 3\%$  overall. In the southern portion of the transect, from the subtropical front through much of the core STW (29 to 39.5°S), the integrated biomasses for protistan grazers and MESO are of comparable magnitudes ( $161 \pm 18$  versus  $187 \pm 25$  mg C m<sup>-2</sup>, respectively). Protistan grazer

- 386 biomass decreases to their lowest levels as MESO biomass increases in the mixing area between
- 387 18.5 and 26°S ( $64 \pm 11$  and  $292 \pm 7$  mg C m<sup>-2</sup>, respectively). Biomass of both protistan grazers
- and MESO are highest in the ITW, averaging  $231 \pm 78$  and  $455 \pm 18$  mg C m<sup>-2</sup>, respectively, in
- 389 waters from 11.5-14°S (Fig. 8b,c).
- 390 3.4. Rate estimates of microbial growth and microzooplankton grazing
- In general, profiles from dilution incubations show low rates of population cell growth and
- microzooplankton grazing mortality in the subtropical front and the STW south of 32°S (Fig. 9).
- Rates tend to be higher at the northern stations, but do not clearly line up with the south-to-north
- trends in latitudinal temperature and light (PAR). For PRO, most upper-EZ growth rate estimates
- north of the subtropical front lie between 0.3-0.6 d<sup>-1</sup>, without a latitudinal trend (Fig. 9a). Grazing
- estimates are generally 0.2-0.5 d<sup>-1</sup>, with occasional surface estimates of 0.7-1.2 d<sup>-1</sup> (Fig. 9e). For
- 397 SYN, upper-EZ growth rates lie between 0.5-0.9 d<sup>-1</sup>, with grazing of 0.2-0.6 d<sup>-1</sup> (Fig. 9b,f). EUK
- 398 growth rates are mostly <0.8 d<sup>-1</sup> and show high incidence of negative growth in the upper EZ at
- many stations, including in the ITW (Fig. 9c). In contrast, EUK grazing estimates are the most
- organized by latitude, with highest values (>1.2 d<sup>-1</sup>) in waters north of 15.5°S (Fig. 9g). With few
- 401 exceptions, growth and grazing rate estimates for HBAC are <0.4 d<sup>-1</sup>, with the bulk 0.2 d<sup>-1</sup> or
- 402 lower (Fig. 9d,h).
- 403 Most growth rate estimates for the phytoplankton community based on Chla vary between
- 404 0.2 and 1.0 d<sup>-1</sup>, with some negative growth rates in the high-light surface incubations and
- subsurface maxima at some stations in the range of 1.2 to 1.6 d<sup>-1</sup> (Fig. 10a). Microzooplankton
- 406 grazing estimates are generally in a similar range, most < 1.0 d<sup>-1</sup> with scattered higher rates up to
- 407 1.7 d<sup>-1</sup> (Fig. 10b). For both growth and grazing estimates, lower rates are concentrated in
- southern stations and higher rates are more evident in the northern transect (Fig. 10a,b).
- 409 *3.5. EZ-integrated production and grazing*
- 410 EZ estimates of phytoplankton carbon production (PROD), calculated from biomass and
- dilution rates, are compared to integrated C estimates of microzooplankton (MICRO) and
- 412 mesozooplankton (MESO) grazing in Figure 11. Based on the sums of FCM-measured
- populations, phytoplankton PROD ranges from 111 to 655 mg C m<sup>-2</sup> d<sup>-1</sup>, increasing relatively
- linearly from 39.5°S through the STW to 27.5°S before leveling off at northern stations (Fig.

- 415 11a). Mean total PROD is  $466 \pm 35$  mg C m<sup>-2</sup> d<sup>-1</sup>. EUK accounts for most of the production
- south of 35°S, while PRO dominates at all other stations. SYN contributes most to PROD (14-
- 417 33%) in the ITW region, although this includes one station (14°S) where integrated EUK PROD
- 418 was a negative value, therefore underestimated, and set to zero for the PROD total. Grazing
- estimates based on the sum of MICRO GRAZ for FCM populations plus MESO GRAZ range
- from 131 to 1071 mg C m<sup>-2</sup> d<sup>-1</sup>, increasing generally from southern to northern stations and
- 421 averaging  $461 \pm 54$  mg C m<sup>-2</sup> d<sup>-1</sup> over the transect. MICRO dominates grazing, accounting for
- 422  $85 \pm 2\%$  on average (range 64-95%).
- Phytoplankton community estimates of PROD based on Chla range from 182 to 1202 mg C
- $d^{-1}$  and average  $d^{-1}$  and average  $d^{-1}$  (Fig. 11b). Station PROD estimates are more irregular
- than for the sum of FCM populations, but the general trend is similar with a south-to-north
- increase leveling off or declining slightly at lower latitudes. Chla-based GRAZ estimates vary
- from 195 to 1272 mg C m<sup>-2</sup> d<sup>-1</sup>, with a transect mean rate of  $604 \pm 80$  mg C m<sup>-2</sup> d<sup>-1</sup>. MICRO
- 428 accounts for  $89 \pm 2\%$  of total GRAZ on average (range 72-97%).
- Integrated estimates of HBAC PROD are approximately an order of magnitude lower than
- 430 for phytoplankton and show a general increasing trend from high-to-low latitude with substantial
- variability between stations (Fig. 11c). HBAC PROD and MICRO GRAZ range from 7 to 196
- and from 10 to 113 mg C m<sup>-2</sup> d<sup>-1</sup>, respectively, with transect averages of  $75 \pm 47$  and  $50 \pm 26$  mg
- 433  $C \text{ m}^{-2} \text{ d}^{-1}$ .
- Although the carbon-based rate estimates from FCM populations are ~25% lower on average
- compared to estimates from Chla, both show strong relationships ( $p<10^{-8}$ ) between PROD and
- 436 GRAZ (Fig. 12a). Slopes for the two relationships are not statistically significant (p>0.35), and
- confidence limits (95%) for both regressions broadly overlap with each other and with the 1:1
- line (FCM = 0.79-1.22; Chla = 0.77-1.12). Thus, both relationships indicate that a general
- balance of phytoplankton production and grazing processes extended over the 110°E transect
- during the period of our investigation. For HBAC, MICRO GRAZ averages ~0.6 \* PROD rates,
- with 95% confidence limits of 0.48-0.72 (Fig. 12b).

## 4. Discussion

- We used complementary methods of flow cytometry, pigment analyses, microscopy,
- 200 zooplankton net sampling and experimental incubations to constrain estimates of microbial

community biomass, C:Chla ratios, growth rates, production and grazing impacts from microand mesozooplankton across the varying water masses of the 110°E transect. For the austral
late-autumn (May-June) period of our investigation, 110°E waters north of the subtropical front
were generally oligotrophic and picophytoplankton dominated, but with substantial south-tonorth gradients in incident light and temperature. These gradients in environmental growth
conditions mainly manifest in increased biomass turnover, measured as carbon-based production
and grazing rates, while integrated biomass of phytoplankton and heterotrophic bacteria show no
consistent trends with latitude. Phytoplankton production and grazing processes are tightly
coupled over the gradient, and biomass accumulates in the higher levels of the food web
(mesozooplankton) at lower latitudes. In the subsections below, we first consider
methodological factors that might influence interpretations of the study results. We then put our
findings in the context of previous results for the eastern Indian Ocean and other open-ocean
low-latitude ecosystems.

## 4.1. Methodological considerations and interpretations

Flow cytometric analyses of cell abundances, fluorescence and light scatter tie together the pigment, biomass and rate components of our study. Where the relationships can be validated, for example, between FCM red fluorescence (RF) and measured Chla (Fig. 3a,b), reasonable agreement is evident. Nonetheless, substantial differences are seen between EZ-integrated RF and TChla in some locations, notably at the southern and northern ends of the transect (Fig. 4c). Among possible explanations, the fact that FCM and HPLC pigment samples are taken from different bottles and depths on the same hydrocast certainly contributes to the variability in comparing individual samples. We expect that FCM subsamples drawn directly from the HPLC water samples would have had lower scatter and higher correlation coefficients than in Figure 3, though not necessarily different depth-integrated estimates based on multiple analyses per profile in Figure 4. For the stations at 11.5 and 12.5°S, however, FCM sampling hit the well-developed DCM peaks whereas the interpolated values from TChla samples missed the DCM. At these stations, therefore, the discrepancies are at least partially explained by sampling underestimates of TChla.

In general, systematic bias can arise where rare large cells exert a disproportionate effect on the mean values of RF (or FALS) in the FCM analyses, which are then applied to all cells in the population. Such circumstances (greater frequency of larger cells) are expected in the southern and northern ends of the transect where nutrient concentrations are higher or the upper nitracline enters the EZ (Figs. 1d,e and 2), and where we observe the largest discrepancies. RF underestimates of TChla, such as those observed at 15.5 and 25.5°S, might also occur where a significant fraction of cells does not survive the preservation, freezing and thawing steps prior to FCM analyses. That might depend on specific taxa or environmental circumstances, however, because, aside from these stations, there is little evidence that we are missing a significant portion of the Chla-containing community. Overall, we attribute most of the discrepancies between RF-based Chla estimates and TChla to the EUK component, which are the more fragile, taxonomically diverse, size-variable and least abundant (least precisely enumerated) cells in the analysis, compared to PRO and SYN.

Our assignments of base values for cell C contents of the FCM-distinguished populations were based on well-used relationships and size scaling but are arbitrary to the extent that different choices would have led to different group contributions to community biomass estimates (Figs. 5 and 7) and different C:Chla values (Fig. 6). Past estimates of C contents range from 15 to 250 fg C cell<sup>-1</sup> for PRO (Moore, 1997; Shalapyonok et al., 2001), 40 to 434 fg C cell<sup>-1</sup> for SYN (Heldal et al., 2003; Casey et al., 2013); 162 to 3980 fg C cell<sup>-1</sup> for EUK (Fuhrman et al., 1989; Worden et al., 2004), and 7.5 to 30 fg C cell<sup>-1</sup> for HBAC (Fukuda et al., 1998; Pomroy and Joint, 1999). Our base values of 32 and 11 fg C cell<sup>-1</sup> for PRO and HBAC, respectively, are based on cell biovolume measurements for open-ocean waters of the Arabian Sea. Our base values for PRO, SYN (155 fg C cell<sup>-1</sup>) and EUK (3150 fg C cell<sup>-1</sup>) also fall within the calibrated cell estimates of Casey et al. (2013) for PRO and SYN in upper EZ waters during summer stratified months (August-October) in the Sargasso Sea, within the calibrated mean annual C estimates for EUK from the same region (Casey et al., 2013), and within the more typical cell C values used in many other studies (Ishizaka et al. 1994; Blanchot and Rodier, 1996; Zubkov et al., 2000; Claustre et al. 2002; Veldhuis and Kraay, 2004).

Relative FALS scaling of cell sizes, as opposed to using fixed cell C values, allows us to account for variability in cell size and biomass with depth and latitude. For the latter, we determined that mean cell C values for the upper EZ ranged from 29 to 39 fg C cell<sup>-1</sup> for PRO and from 129 to 214 fg C cell<sup>-1</sup> for SYN, both with declining south-to-north trends (Landry et al., 2022). HBAC ranged narrowly around 11 fg C cell<sup>-1</sup> at all stations while upper EZ mean C for

EUK varied from a minimum of ~2000 fg C cell<sup>-1</sup> at 12.5-14°S to a maximum of 4200-4600 fg C cell<sup>-1</sup> at 17-18°S. For depth variability, we found that cell size variability at individual stations was consistently low in the upper EZ above 7.6% Io, where the water column was well mixed (Landry et al., 2022). However, PRO and SYN cells in the deep EZ were significantly larger than surface cells (>12% and up to 150% greater C) at all stations north of 29°S, except 14 and 15.5°S. These coincide, for the most part, to stations where a DCM was evident (Fig. 1). HBAC did not show notable depth variability in cell C at any station, and EUK cells in the deep EZ were always similar to or up to 50% smaller than cell sizes of surface samples, whereas deeper PRO and SYN cells were larger than surface cells. Thus, in the absence of measurements for each population at each depth, there are no general corrections for depth or latitudinal variability that would be applicable to cell sizes of all populations. The C:Chla profiles in Figure 6 incorporate all of the measured cell variability in RF and FALS. Consequently, absolute values would change with different assumptions about base cell

FALS. Consequently, absolute values would change with different assumptions about base cell C estimates, but the relative station differences would remain robust. For cells experiencing consistently high PAR in the upper EZ (i.e., stations north of 26°S; Table 1), the variability in C:Chla ratios can be reasonably viewed as relating to varying degrees of nutrient (N) limitation (Geider et al., 1997; Taylor et al., 1997). Adopting that interpretation here, the profiles from 20-21.5°S with the highest C:Chla define the area of strongest nutrient limitation for all populations, with 17-18.5°S also high from PRO and 11.5°S high for SYN and EUK.

Individual rate estimates from dilution experiments (Fig. 9 and 10) come from paired unreplicated bottles, and thus incorporate random errors that are at least partially averaged out in the EZ-integrated rate estimates and latitudinal trends (Fig. 11). With regard to possible biases or artifacts, one concern is the timing of experiments, which were setup less-than-ideally in the evening when some populations undergo semi-synchronous cell division (Vaulot, 1992; Vaulot et al. 1995; Liu et al., 1998). Thus, growth rate estimates may have some carryover effect from the prior daylight period in addition to the light conditions experienced during the full day of incubation. Also, if incubation conditions delay or advance cell division cycles relative to those experienced in the water column, that could lead to under- or over-estimates of growth relative to grazing over the 24-h period. We note, for example, that cell growth rates and microzooplankton grazing estimates are not in perfect balance for bacterial populations, as they are in some studies (e.g., Landry et al. 2011, 2016b). For PRO and HBAC, the mean net growth rates over the

integrated EZ are relatively small  $(0.06 \pm 0.06 \text{ and } 0.05 \pm 0.02 \text{ d}^{-1}$ , respectively) and might reasonably be explained by either direct or indirect impacts of the missing mesozooplankton predation in the incubation experiments. Direct mesozooplankton grazing on bacteria-sized particles is expected from appendicularians, which were abundant along the transect, comprising 11-23% of the mixed-layer zooplankton collected by a towed Continuous Plankton Recorder in water north of the subtropical front (Davies et al., this volume). Appendicularians also have substantially (up to 10X) higher clearance rates than suspension-feeding copepods of similar biomass (Alldredge, 1981). Based on measured clearance rates of Oikopleura fusifomis on bacteria in a subtropical estuary (Scheinberg et al., 2005), water-column densities of one appendicularian per 15-18 L would be sufficient to account fully for the grazing on PRO and HBAC not provided by microzooplankton. In addition, the absence of mesozooplankton predation on large microzooplankton (ciliates and large dinoflagellates) in the incubations can indirectly cascade to lower levels via elevated grazing on intermediate EUK-sized consumers, which reduces grazing on bacteria. First et al. (2009) observed, for example, that their results from size-fractioned dilution experiments in oligotrophic waters of the Gulf of Mexico could be reproduced by cascading trophic interactions in a model with three interacting consumers. Compared to PRO and HBAC, the net rate differentials between growth and microzooplankton grazing for SYN and EUK are more substantial and in opposite directions  $(+0.31 \pm 0.3 \text{ versus } -0.29 \pm 0.9 \text{ d}^{-1}$ , respectively). For SYN, which contributes relatively little to total community production and grazing (Fig. 11), the large net growth discrepancy implies either that growth rates might be overestimated, possibly by an acceleration of cell division by experimental timing or incubation conditions, or that we are missing an important EZ loss term from the incubation bottles. SYN is notable among pico-phytoplankton in being strongly linked to export processes (Amacher et al., 2013; Guidi et al., 2016) as well as being resistant to digestion by metazoan consumers (Johnson et al., 1982; Pfannkuche and Lochte, 1993; Gorsky et al., 1999; Wilson and Steinberg, 2010; Stukel et al., 2013). Aggregate formation has been hypothesized as a mechanism that both facilitates SYN sinking as well as increases their availability to mesozooplankton grazers which concentrates undigested SYN into fast sinking pellets (Agustí et al., 2015; Deng et al., 2016; Stukel et al., 2013). Metagenomic studies have also demonstrated very substantial differences in export contributions of SYN clades compared

537

538

539

540

541

542

543

544

545

546

547

548

549

550

551

552

553

554

555

556

557

558

559

560

561

562

563

564

565

566

567

to their relative abundances in the water column (e.g., De Martini et al., 2018; Valencia et al.,

2021). Our observed decoupling of growth and microzooplankton grazing rates for SYN in incubation experiments might therefore be indicative of an outsized role of local strains in export, possibly combined with digestion resistance to grazing by some protists such that cells disappear from FCM analyses at a lower rate than they are actually consumed.

For EUK, the high growth rate variability and substantial negative rates found in locations with temperatures of 27-28°C (Figs. 9, 11a) are consistent with viral infection or spontaneous lysis, which have been reported more prevalent for picoeukaryotes than photosynthetic bacteria and exacerbated by high light and temperature (Agustí and Sánchez 2002; Baudoux et al., 2007: 2008; Bidle, 2016). As noted by Landry et al. (2022), the declines in our experiments were not triggered by abrupt differences in light or temperature between collection and incubation days (Table 1), and they occurred in bottles that had not been screened, filtered or manipulated in any way other than gentle filling. However, the light conditions experienced by cells held at high light for the full photoperiod in deck incubators clearly differed from the average conditions experienced in a freely mixed water column, which may have led, for example, to weakened cells in the experiments more likely to lyse during sample preservation, freezing and thawing prior to FCM analysis. Thus, it is not clear whether EUK cells were lost during the incubation or in post-experiment handling. In this regard, it is tempting to consider the FCM-based analyses of production and grazing as likely more accurate that the Chla-based estimates, because the former are based on relatively precise enumerations of individual cells while the latter have pigment corrections. Considering the issues on both sides, we view the FCM- and Chla-based analyses as providing equally valid or flawed representations, as the case may be, of community growth and grazing rates. The power of combining these approaches in the present study is that they give mutually supportive trends and relationships.

## 4.2. Plankton dynamics of the eastern Indian Ocean

568

569

570

571

572

573

574

575

576

577

578

579

580

581

582

583

584

585

586

587

588

589

590

591

592

593

594

595

596

597

The historic IIOE sampling along 110°E in 1962-63 was the first integrated investigation of circulation, nutrients, primary productivity and zooplankton in the eastern Indian Ocean (Jitts, 1969; Humphrey and Kerr, 1969: Newell, 1969: Rochford, 1969, 1977; Tranter, 1977a,b; Tranter and Kerr, 1969, 1977) and here provides the broader seasonal and spatial context for our May-June cruise results. According to Jitts (1969), May-June coincides with the seasonal transition to high primary production (beginning of the austral winter SE monsoon), which persists from mid-

598 May to October in tropical waters north of 15°S but develops later and has shorter duration (mid-599 June through August) in subtropical waters at 30-32°S (IIOE sampling did not extend to the 600 subtropical front). Part of the production gradient that we observe between southern and 601 northern ends of the transect is therefore explained by the timing and sampling direction of the 602 2019 cruise, which began during a period of moderate primary production in the south and ended 603 during the higher production season in the north. During the relevant time periods, the noon-to-604 sunset <sup>14</sup>C incubations of Jitts (1969) under simulated in situ light conditions averaged 69 mg C m<sup>-2</sup> h<sup>-1</sup> for <15°S stations and 24 mg C m<sup>-2</sup> h<sup>-1</sup> for 30-32°S, which correspond to daily rates of 605 606 828 and 288 mg C m<sup>-2</sup> d<sup>-1</sup>, respectively, assuming sustained rates over a 12-h photoperiod. 607 These values are reasonably close to 24-h production estimates from the present experiments at 608 latitudes <15.5°S (578  $\pm$  56 and 793  $\pm$  122 mg C m<sup>-2</sup> d<sup>-1</sup> for FCM and Chla-based rates, 609 respectively) but a little lower than our estimates for STW  $> 30^{\circ}$ S (388  $\pm$  11 and 472  $\pm$  128 mg C m<sup>-2</sup> d<sup>-1</sup>). Given that historical estimates of <sup>14</sup>C uptake often underestimate the rates from 610 611 contemporary measurements by a factor of 2 or more (Marra and Heinemann, 1987), the good 612 agreement here might be attributed to 110°E IIOE investigators being ahead of their time in 613 recognizing and mitigating poisoning effects during seawater collection and using blue filters to 614 simulate deep-EZ light conditions (Jitts, 1963, 1969). On the other hand, significant IIOE rate 615 underestimates due to historical methodological issues could also be masking any evidence of 616 diminished production over the past six decades. The available data does not allow us to 617 distinguish between these alternatives. 618 IIOE sampling shows two seasonal peaks of mesozooplankton biomass, with May-June being 619 a low period between them (Tranter and Kerr, 1969). The major zooplankton peak occurs in 620 August-September (~2-4 X May-June biomass) during the late SE monsoon, and the minor peak 621 occurs in February-March in the late phase of the austral summer NW monsoon. Despite the 622 seasonal trends, the latitudinal gradient from low mesozooplankton biomass south of 26°S 623 (STW) to high biomass north of 14°S (ITW) (Fig. 8c) remains a fairly consistent year-long 624 feature of the study region (Tranter and Kerr, 1977). However, the biomass structure also 625 includes variability in the types and timing of macrozooplankton and micronekton, the 626 presumptive predators of mesozooplankton sampled by large trawl nets, which in general lag the 627 peak biomass of mesozooplankton by 2-3 months (Legand, 1969). Based on these IIOE 628 timelines, we frame our cruise as capturing the onset of elevated primary productivity in tropical-

629 subtropical waters associated with the SE monsoon, during which mesozooplankton biomass will 630 accumulate to be eventually overtaken by a later peak of larger predators. For our most southern 631 stations in the subtropical front that were not sampled during IIOE, our cruise clearly occurred 632 during a period of seasonal cooling and deeper mixing when light, rather than nutrients, provides 633 the major constraint on productivity and dilution decreases grazing (Sverdrup, 1953; Behrenfeld, 634 2010). 635 Recent studies in the eastern IO have focused on the impacts of mesoscale eddies on 636 productivity, zooplankton and fishery recruitment (Strzelecki et al., 2007; Waite et al., 2007b, 637 2019; Wang et al., 2014; Säwström et al., 2014) or the Leeuwin Current region further to the east 638 (Thompson et al., 2012; Lourey et al., 2013; Sutton and Beckley, 2016). The center areas of the 639 anticyclonic warm-core eddies that form off western Australia are Leeuwin Current water, with 640 the tropical signature of lower salinity as well as some coastal phytoplankton (diatom) influences 641 (Feng et al., 2007; Paterson et al., 2007). In Waite et al. (2007a), two eddies sampled in the 642 vicinity of 31-32°S, 110°E in October, the end of the SE monsoon, differed 2-fold in integrated 643 <sup>14</sup>C primary production, with the warm-core eddy higher in productivity (400 versus 240 mg C 644 m<sup>-2</sup> d<sup>-1</sup>) as well as zooplankton biomass (780 versus 390 mg C m<sup>-2</sup>; Strzelecki et al., 2007) than the cold-core eddy. The production values fall within our 190-808 mg C m<sup>-2</sup> d<sup>-1</sup> estimates for 645 646 integrated production in the 30.5-33.5°S region (Fig. 11), but our averages ( $404 \pm 16$  and  $436 \pm 16$ 647 189 mg C m<sup>-2</sup> d<sup>-1</sup> for FCM and Chla, respectively) are closer to the higher warm-core eddy rates. Our zooplankton biomass estimates in this latitudinal range ( $283 \pm 12 \text{ mg C m}^{-2}$ ) are lower than 648 649 both the warm- and cold-core eddy estimates of Strzelecki et al. (2007), which were sampled to a 650 deeper (150 m) depth and later in the high production season when mesozooplankton biomass 651 has accumulated and shifted to predominately carnivorous taxa (60-70% carnivores; Strzelecki et 652 al., 2007). 653 To our knowledge, there are no previous grazing estimates for mesozooplankton along the 654 110°E transect, but microzooplankton grazing was measured in the eddy studies as well as at 655 three stations across the Leeuwin Current (Paterson et al., 2007, 2008). Paterson et al. (2007) 656 found that microzooplankton consumed all or most phytoplankton production in both eddy types, 657 with large dinoflagellates the major grazers in the warm-core eddy while ciliates dominated in 658 the cold-core eddy. In seasonal experiments conducted with surface water samples from a

coastal lagoon to the continental slope, microzooplankton consumption generally balanced cell

growth of FCM-measured picoplankton populations at all times and stations, while Chla-based rates exhibited substantial positive net growth, though uncorrected for photoacclimation effects (Paterson et al., 2008). To the extent that comparisons can be made, these prior results are consistent with the present finding of a relatively close coupling of production and grazing processes, with the latter provided mainly by microzooplankton.

#### 4.3. Comparisons to other subtropical and tropical ecosystems

660

661

662

663

664

665

666

667

668

669

670

671

672

673

674

675

676

677

678

679

680

681

682

683

684

685

686

687

688

689

In Table 2, we compare the ranges of measured EZ characteristics along the 110°E transect to those of other low-latitude, warm-water ecosystems that have been investigated by similar methods. Despite occupying a distinctly different latitudinal range, the 110°E stations compare particularly well to the equatorial Pacific in EZ depth, integrated TChla, production and grazing. The microzooplankton biomass for 110°E is lower relative to other systems because heterotrophic flagellates (other than >5-µm dinoflagellates), often comprising half or more of that biomass, were not enumerated in the present study. The lower mesozooplankton biomass and grazing is explained by our sampling during the 110°E seasonal mesozooplankton minimum. The equatorial Pacific upwelling system is a meaningful basis of comparison to the present results because an inverse network model for that region incorporating mean values and uncertainties for experimental rate profiles was consistent with many of the system's independently measured parameters and fully explained how trophic flows originating from small phytoplankton and microzooplankton-dominated grazing supported high growth rates of mesozooplankton (Landry et al., 2020b). While such an analysis is beyond the scope of the present study, it is reasonable to expect that similar trophic interactions might also apply in the eastern IO. There are, however, substantial differences between the two regions in the structure and composition of the phytoplankton communities. Notably, flagellates have a major role in the equatorial Pacific, with PRO and diatoms making lesser and approximately equal (18%) contributions to production (Landry et al., 2011).

New production in the equatorial Pacific derives from Trade Wind divergent upwelling on the equator, while the ITF is a major source of new nutrients to the eastern IO (Ayers et al., 2014), which shifts the location of nutrient-enhanced tropical waters substantially to the south. In addition, strong wind-driven upwelling along the southern coast of Indonesia during the SE monsoon forms a prominent thermocline dome (Java Dome) where the westward flowing South

690 Equatorial Current takes an anticyclonic turn (Wyrti, 1962). The original 110°E IIOE 691 investigations extended to 9.5°S, approximately a degree south of the Java Dome upwelling. The seasonal mesozooplankton biomass maximum there is 5200 mg C m<sup>-2</sup> during the SE 692 693 monsoon (July and August), based on conversion of wet weight data from Tranter and Kerr 694 (1969) to carbon equivalents and correcting for mesh size (333 µm to 200 µm) according to 695 Moriarty and O'Brien (2013). Table 2 therefore misses the upper range of values along 110°E 696 that can be compared to systems with highly seasonal dynamics. For example, the maximum 697 values of biomass, production and grazing for the Arabian Sea in Table 2 are from the SW 698 monsoon upwelling season in August, and the eastern tropical Pacific study sampled the Costa 699 Rica Dome, an analogous thermocline-ridge feature to the Java Dome (Wyrti, 1964), during the 700 summer upwelling peak (Landry et al., 2016a). We might expect, therefore, that the far northern 701 edge of the 110°E transect has a seasonally shallow and rich EZ that supports biomass and 702 production levels similar to or approaching those of the Arabian Sea and Costa Rica Dome. 703 Such a region would reasonably have a phytoplankton community with much higher 704 contributions of large phytoplankton cells (diatoms and dinoflagellates) than we found in the 705 present study at the beginning of the high production season. 706 On the other extreme, the open waters of the Gulf of Mexico sampled during the springtime 707 (Girard et al., in review) are less productive than the mean state of the eastern IO during our 708 sampling in late austral fall, but have stronger similarities in phytoplankton community 709 composition, including PRO dominance of biomass and production (40-65%), with relatively 710 minor roles for diatoms and dinoflagellates (Landry et al., 2021; Selph et al., 2021a). 711 Prymnesiophytes appear to play a dominant role among eukaryotic phytoplankton in the Gulf of 712 Mexico, which might also be the case along 110°E based on similarities the percent contributions 713 of 19'-hexanoyloxyfucoxanthin, the prymnesiophyte-associated pigment, to total concentration 714 of taxon-diagnostic eukaryotic carotenoids (57.9  $\pm$  0.6%, Gulf of Mexico; Selph et al. 2021a 715 versus  $54.7 \pm 0.5\%$ ; D. Antoine, unpubl.). Thus, most of the cells enumerated as EUK in our 716 FCM analyses are likely small prymnesiophytes. Careful analysis of the oceanic subregion of

appear to be sustained by subsidies of fixed production and zooplankton transported by mesoscale eddies to open waters from the outer edges of the continental margins (Kelly et al.,

the Gulf of Mexico has further shown insufficient nutrient fluxes and *in situ* productivity to

support the measured zooplankton biomass and loss rate of EZ organics due to export. Both

717

718

719

- 2021; Landry and Swalethorp, 2021). Tranter and Kerr (1977) suggested something similar to
   explain the observed zooplankton biomass maximum in subtropical waters along 110°E during
   the SE monsoon, arguing that it was spatially decoupled from tropical upwelling in the Java
   Dome and more likely came from a closer coastal upwelling source along northwestern Australia
- 725 (Rossi et al., 2003).

726

727

728

729

730

731

732

733

734

735

736

737

738

739

740

741

742

743

744

745

746

747

748

749

750

## 5. Summary and conclusions

We investigated plankton community structure and food-web dynamics from bacteria to mesozooplankton along the historic IIOE 110°E transect with the goals of 1) identifying key characteristics of its system-level trophic relationships for ecosystem modeling, 2) evaluating possible climate-driven changes in productivity since its last major study in the 1960s, 3) comparing 110°E to other similarly studied open-ocean regions. For general system characteristics, picophytoplankton, especially *Prochlorococcus*, dominated production, and microzooplankton dominated grazing, with total phytoplankton production and grazing processes tightly coupled over the transect. Strong south-to-north gradients in incident light and temperature during our sampling period had relatively little systematic effect on distributions of phytoplankton and bacterial biomass over the transect, but turnover rates (production and grazing) as well as mesozooplankton biomass displayed significant latitudinal trends. Our May-June cruise sampled the system as it was previously described, during the seasonal minimum of mesozooplankton biomass and transition to high primary productivity at the northern end. Although early methods may have underestimated productivity during IIOE, thereby masking a climate-driven decline, our contemporary estimates are similar in magnitude to the values reported for monthly estimates then and thus provide little evidence of change. While we are missing data during the periods and locations of maximum biomass accumulation to compare to other highly seasonal low-latitude systems (Arabian Sea, Costa Rica Dome) during their seasonal peaks, stocks and rate relationships along 110°C are comparable to results from other ecosystems. Rate similarities are notable between the tropical ITF waters and central equatorial Pacific upwelling area, but phytoplankton community structure is more similar to the oceanic Gulf of Mexico. These mixed system characteristics may reflect sampling during the seasonal production transition and would be useful to corroborate during the period of peak SE monsoon forcing (August-September).

## **Declaration of competing interest**

The authors declare that they have no known competing financial interests or personal relationships that could appear to influence the work reported in this paper.

#### **Acknowledgements**

751

754

755

756

757

758

759

760

761

762

763

764

765

766

767

768

769

770

771

772

773

774

775

776

777

778

We thank the CSIRO Marine National Facility (MNF) for its support in the form of sea time on R/V *Investigator*, support personnel, scientific equipment and data management. We especially acknowledge the CSIRO hydrography/hydrochemistry team for their exceptional efforts in providing CTD and nutrient data. Greg Mitchell and Elliot Weiss provided optical expertise for the construction and calibration of the incubator boxes. Phytoplankton pigment analyses were performed by Céline Dimier and Joséphine Ras from the "Service d'Analyses de Pigments par HPLC" (SAPIGH) analytical platform of the Institut de la Mer de Villefranche (CNRS-France). Kelsey Fleming and Rasmus Swalethorp assisted with imaging and data analyses of microscopy samples. Research support was provided by National Science Foundation Grant OCE-1851558, a Murdoch University Distinguished Collaborator Award, the Hong Kong Branch of Southern Marine Science and Engineering Guangdong Laboratory (Guangzhou; SMSEGL20SC02), and the European Space Agency (PO N 5001026051). Water and plankton samples at 29-23°S, 110°E were taken under Australian Fisheries Management Authority scientific permit 1004152, Australian Government permit AU-COM2019-446 and those in the Abrolhos Marine Park under permit PA2018-00065-1 issued by the Director of National Parks, Australia. All data from the voyage are publicly available in accordance with MNF Policy. The views expressed in this publication do not necessarily represent those of the Director of National Parks, CSIRO or the Australian Government.

#### **Author statement**

M.R.L. and L.E.B. conceived the study. M.R.L., R.R.H., C.H.D. and D.A. conducted the field sampling and experiments. K.E.S. did the flow cytometric analyses; D.A. contributed the HPLC pigment analyses; and M.K. analyzed the microscopy samples. M.R.L. analyzed results and drafted the manuscript. All authors contributed to comments and edits of the manuscript.

- 779 References
- 780 Agustí, S., González-Gordillo, J.I., Vaqué, D., Estrada, M., Cerezo, M.I., Salazar, G., Gasol, J.M.,
- Duarte, C.M., 2015. Ubiquitous healthy diatoms in the deep sea confirm deep carbon injection
- by the biological pump. Nat. Commun. 6, doi:10.1038/ncomms8608.
- Agustí, S., Sánchez, M.C. 2002. Cell viability in natural phytoplankton communities quantified by a
- membrane permeability probe. Limnol. Oceanogr. 47, 818–828.
- Alldredge, A.L. 1981. The impact of appendicularian grazing on natural food concentrations in situ.
- 786 Limnol. Oceanogr. 26, 247-257.
- Amacher, J., Neuer, S., Lomas, M., 2013. DNA-based molecular fingerprinting of eukaryotic protists
- and cyanobacteria contributing to sinking particle flux at the Bermuda Atlantic time-series study.
- 789 Deep Sea Res II 93, 71–83.
- Ayers, J.M., Strutton, P.G., Coles, V.J., Hood, R.R., Matear, R.J., 2014. Indonesian throughflow
- nutrient fluxes and their potential impact on Indian Ocean productivity. Geophys. Res. Lett. 41,
- 792 5060–506.
- Azam, F., Fenchel, T., Field, G.J., Gray, J.S., Meyer-Reil, L.A., Thingstad, F., 1983. The ecological
- role of water-column microbes in the sea. Mar. Ecol. Prog. Ser. 10: 257–263.
- Balch, W.M., Poulton, A.J., Drapeau, D.T., Bowler, B.C., Windecker, L.A., Booth, E.S., 2011.
- Zonal and meridional patterns of phytoplankton biomass and carbon fixation in the Equatorial
- Pacific Ocean between 110°W and 140°W. Deep-Sea Res II 58, 400–416.
- Barber, R.T., Marra, J., Bidigare, R., Codispoti, L., Halpern, D., Johnson, Z., Latasa, M., Goericke,
- R., Smith, S., 2001. Primary productivity and its regulation in the Arabian Sea during 1995.
- 800 Deep Sea Res. II 48, 1127–1172.
- Baudoux, A.C., Veldhuis, M.J.W., Noordeloos, A.A.M., van Noort, G., Brussaard, C.P.D., 2008.
- 802 Estimates of virus vs. grazing induced mortality of picophytoplankton in the North Sea during
- 803 summer. Aquat. Microb. Ecol. 52, 69–82.
- Baudoux, A.C., Veldhuis, M.J., Witte, H.J., Brussaard, C.P., 2007. Viruses as mortality agents of
- picophytoplankton in the deep chlorophyll maximum layer during IRONAGES III. Limnol.
- 806 Oceanogr. 52, 2519–2529.

- 807 Beckley, L.E., Thompson, P.A., Hood, R.R. This volume. Revisiting 110°E: A coupled bio-physical,
- 808 ecosystem-scale examination of Australia's International Indian Ocean Expedition line. Deep-
- Sea Res. II (in prep).
- 810 Behrenfeld, M.J., 2010. Abandoning Sverdrup's Critical Depth Hypothesis on phytoplankton
- 811 blooms. Ecology 91, 977–989.
- Bidle, K.D., 2016. Programmed cell death in unicellular phytoplankton. Current Biol. 26, R594–
- 813 R607, doi:10.1016/j.cub.2016.05.056.
- Blanchot, J., Rodier, M., 1996. Picophytoplankton abundance and biomass in the western tropical
- Pacific Ocean during the 1992 El Niño year: results from flow cytometry. Deep-Sea Res. I 43,
- 816 877–895.
- Calbet, A., Landry, M.R., 2004. Phytoplankton growth, microzooplankton grazing and carbon
- cycling in marine systems. Limnol. Oceanogr. 49, 51–57.
- Caron, D.A., Dennett, M.R., 1999. Phytoplankton growth and mortality during the 1995 Northeast
- Monsoon and Spring Intermonsoon in the Arabian Sea. Deep Sea Res. II 46, 1665–1690.
- 821 Casey, J.R., Aucan, J.P., Goldberg, S.R., Lomas, M.W., 2013. Changes in partitioning of carbon
- amongst photosynthetic pico- and nano-plankton groups in the Sargasso Sea in response to
- changes in the North Atlantic Oscillation. Deep-Sea Res. II 93, 58–70.
- Chisholm, S.W., Olson, R.J., Zettler, E.R., Waterbury, J., Goericke, R., Welschmeyer, N., 1988. A
- novel free-living prochlorophyte occurs at high cell concentrations in the oceanic euphotic zone.
- 826 Nature 334, 340–343.
- Claustre, H., Bricaud, A., Babin, M., Bruyant, F., Guillou, L., Le Gall, F., Marie, D., Partensky, F.,
- 828 2002. Diel variations in *Prochlorococcus* optical properties. Limnol. Oceanogr. 47, 1637-1647.
- Davies, C.H., Beckley, L.E., Richardson, A.J., This volume. Are zooplankton assemblages defined
- by water masses along 110°E, Indian Ocean? Deep-Sea Res. II (in prep.).
- Décima M., Landry, M.R., Rykaczewski, R.R., 2011. Broad-scale patterns in mesozooplankton
- biomass and grazing in the eastern equatorial Pacific. Deep-Sea Res II 58, 387–400.
- Décima, M., Landry, M.R., Stukel, M.R., Lopez-Lopez, L., Krause, J.W., 2016. Mesozooplankton
- biomass and grazing in the Costa Rica Dome: amplifying variability through the plankton food
- web. J. Plankton Res. 38, 317–330.

- De Martini, F., Neuer, S., Hamill, D., Robidart, J., Lomas, M.W., 2018. Clade and strain specific
- contributions of *Synechococcus* and *Prochlorococcus* to carbon export in the Sargasso Sea.
- 838 Limnol Oceanogr 63, S448–S457.
- Deng, W., Cruz, B.N., Neuer, S., 2016. Effects of nutrient limitation on cell growth, TEP production
- and aggregate formation of marine *Synechococcus*. Aquat. Microb. Ecol. 78, 39–49.
- Desbruyères, D., McDonagh, E.L., King, B.A., Thierry, V., 2017. Global and full-depth ocean
- temperature trends during the early 21st century from Argo and repeat hydrography. J. Clim. 30,
- 843 1985–1997.
- DuRand, M.D., Olson, R.J., 1996. Contributions of phytoplankton light scattering and cell
- concentration changes to diel variations in beam attenuation in the equatorial Pacific from flow
- cytometric measurements of pico-, ultra- and nanoplankton. Deep Sea Res. II 43, 891–906.
- 847 Feng, M., Majewski, L.J., Fandry, C.B., Waite, A.M., 2007. Characteristics of two counter-rotating
- eddies in the Leeuwin Current system off the Western Australian coast. Deep-Sea Res. II 54,
- 849 961–980.
- First, M.A., Miller III, H.L., Lavrentyev, P.J., Pinckney, J.L., Burd, A.B., 2009. Effects of
- microzooplankton growth and trophic interactions on herbivory in coastal and offshore
- environments. Aquat. Microb. Ecol. 54, 255–267.
- Freibott, A., Taylor, A.G., Selph, K.E., Liu, H., Zhang, W., Landry, M.R., 2016. Biomass and
- composition of protistan grazers and heterotrophic bacteria in the Costa Rica Dome during
- summer 2010. J. Plankton Res. 38, 230–243.
- Fuhrman, J.A., Sleeter, T.D., Carlson, C.A., Proctor, L.M., 1989. Dominance of bacterial biomass in
- the Sargasso Sea and its ecological implications. Mar. Ecol. Prog. Ser. 57, 207–217.
- Fukuda, R., Ogawa, H., Nagata, T., Koike, I., 1998. Direct determination of carbon and nitrogen
- contents of natural bacterial assemblages in marine environments. Appl. Environ. Microbiol. 64,
- 860 3352–3358.
- Garrison, D.L., Gowing, M.M., Hughes, M.P., Campbell, L., Caron, D.A., Dennett, M.R.,
- Shalapyonok, A., Olson, R.J., Landry, M.R., Brown, S.L., Liu, H.-B., Azam, F., Steward, G.F.,
- Ducklow, H.W., Smith, D.C., 2000. Microbial food web structure in the Arabian Sea: a US
- 364 JGOFS study. Deep-Sea Res. II 47, 1387–1422.

- Geider, R.J., MacIntyre, H.L., Kana, T.M., 1997. A dynamic model of phytoplankton growth and
- acclimation: responses of the balanced growth rate and the chlorophyll a:carbon ratio to light,
- nutrient-limitation and temperature. Mar. Ecol. Prog. Ser. 148, 187–200.
- 688 Gifford, D.J., 1988. Impact of grazing by microzooplankton in the Northwest Arm of Halifax
- Harbour, Nova Scotia. Mar. Ecol. Prog. Ser. 47, 249–258.
- 670 Gorsky, G, Chrétiennot-Dinet, M.J., Blanchot, J., Palazzoli, I., 1999. Picoplankton and nanoplankton
- aggregation by appendicularians: Fecal pellet contents of *Megalocerus huxleyi* in the equatorial
- Pacific. J. Geophys. Res. 104, 3381–3390.
- 673 Gregg, W.W., Rousseux, C.S., 2019. Global ocean primary production trends in the modern ocean
- 874 color satellite record (1998-2015). Environ. Res. Lett. 14, 124011, doi:10.1088/1748-
- 9326/ab4667.
- 676 Guidi, L., Chaffron, S., Bittner, L., Eveillard, D., Larhlimi, A., Roux, S., Darzi, Y., Audic, S.,
- Berline, L., Brum, J.R., Coelho, L.P., Espinoza, J.C.I., Malviya, S., Sunagawa, S., Dimier, C.,
- Kandels-Lewis, S., Picheral, M., Poulain, J., Searson, S., *Tara* Oceans Consortium Coordinators,
- Stemmann, L., Not, F., Hingamp, P., Speich, S., Follows, M., Karp-Boss, L., Boss, E., Ogata, H.,
- Pesant, S., Weissenbach, J., Wincker, P., Acinas, S.G., Bork, P., de Vargas, C., Iudicone, D.,
- Sullivan, M.B., Raes, J., Karsenti, E., Bowler, C., Gorsky, G., 2016. Plankton networks driving
- carbon export in the oligotrophic ocean. Nature 532, 465–470.
- Humphrey, G.F., Kerr, J.D., 1969. Seasonal variation in the Indian Ocean along 110°E. III.
- Chlorophylls a and c. Aust. J. Mar. Freshwater Res. 20, 55–64.
- 885 Irigoien, X., 1998. Gut clearance rate constant, temperature and initial gut contents: a review. J.
- 886 Plankton Res. 20, 997–1003.
- Ishizaka. J., Kiyosawa, H., Ishida, K., Ishikawa, K., Takahashi, M., 1994. Meridional distribution
- and carbon biomass of autotrophic picoplankton in the Central North Pacific Ocean during late
- northern summer 1990. Deep-Sea Res. I 41, 1745–1766.
- Jitts H.R., 1963. The simulated in situ measurement of oceanic primary production. Aust. J. Mar.
- Freshwater Res. 14, 139–147.
- Jitts, H.R., 1969. Seasonal variation in the Indian Ocean along 110°E. IV. Primary production. Aust.
- 893 J. Mar. Freshwater Res. 20, 65–75.

- Johnson, P.W., Huai-Shu, X., Sieburth, J.M., 1982. The utilization of chroococcoid cyanobacteria by
- marine protozooplankters but not by calanoid copepods. Ann. Inst. Oceanogr. Paris Nouv. Ser.
- 896 58, 297–308.
- Kelly, T.B., Landry, M.R., Selph, K.E., Knapp, A.N., Swalethorp, R., Stukel, M.R., 2021. Lateral
- advection supports nitrogen export in the oligotrophic open-ocean Gulf of Mexico. Nature
- 899 Comm., 12:332, doi.org/10.1038/s41467-021-23678-9.
- 200 Landry, M.R., 2009. Grazing processes and secondary production in the Arabian Sea: A simple food
- web synthesis with measurement constraints. *In*: Wiggert, J.R., Hood, R.R., Naqvi, S.W.A.,
- Brink, K.H., Smith, S,L. (eds.), Indian Ocean: Biogeochemical Processes and Ecological
- 903 Variability. AGU Monograph Series 185, 133–146.
- Landry, M.R., Brown, S.L., Campbell, L., Constantinou, J., Liu, H., 1998. Spatial patterns in
- 905 phytoplankton growth and microzooplankton grazing in the Arabian Sea during monsoon
- 906 forcing. Deep-Sea Res. II 45, 2353–2368.
- Landry, M.R., Brown, S.L., Neveux, J., Dupouy, C., Blanchot, J., Christensen, S., Bidigare, R.R.,
- 2003. Phytoplankton growth and microzooplankton grazing in high-nutrient, low-chlorophyll
- waters of the equatorial Pacific: Community and taxon-specific rate assessments from pigment
- and flow cytometric analyses. J. Geophys. Res. 108, C12, 8142, doi:10.1029/2000JC000744.
- Landry, M.R., Brown, S.L., Rii, Y.M., Selph, K.E., Bidigare, R.R., Yang E.J., Simmons, M.P., 2008.
- Depth-stratified phytoplankton dynamics in Cyclone *Opal*, a subtropical mesoscale eddy. Deep-
- 913 Sea Res. II 55, 1348–1359.
- Landry, M.R., De Verneil, A., Goes, J.I., Moffett, J.W., 2016a. Plankton dynamics and
- biogeochemical fluxes in the Costa Rica Dome: Introduction to the CRD Flux and Zinc
- 916 Experiments. J. Plankton Res. 38, 167–182.
- Landry, M.R., Hood, R.R., Davies, C.H., 2020a. Mesozooplankton biomass and temperature-
- enhanced grazing along a 110°E transect in the eastern Indian Ocean. Mar. Ecol. Prog. Ser. 649,
- 919 1–19.
- 920 Landry, M.R., Selph, K.E., Décima, M., Gutiérrez-Rodríguez, A., Stukel, M.R., Taylor, A.G.,
- Pasulka, A.L., 2016b. Phytoplankton production and grazing balances in the Costa Rica Dome. J.
- 922 Plankton Res. 38, 366–379.

- Landry, M.R., Selph, K.E., Hood, R.R., Davies, C.H., Beckley, L.E., In review. Low temperature
- sensitivity of picophytoplankton P:B ratios and growth rates across a natural 10°C temperature
- gradient in the oligotrophic Indian Ocean. Limnol. Oceanogr. Lett.
- Landry, M.R., Selph, K.E., Stukel, M.R., Swalethorp, R., Kelly, T.B., Beatty, J., Quackenbush, C.R.,
- 927 2021. Microbial food web dynamics in the oceanic Gulf of Mexico. J. Plankton. Res. 1-18,
- 928 doi:10.1093/plankt/fbab021.
- Landry, M.R., Selph, K.E., Taylor, A.G., Décima, M., Balch, W.M. and Bidigare, R.R., 2011a.
- Phytoplankton growth, grazing and production balances in the HNLC equatorial Pacific. Deep-
- 931 Sea Res. II 58, 524–535.
- Landry, M.R., Stukel, M.R., Décima, M., 2020b. Food-web fluxes support high rates of
- mesozooplankton respiration and production in the equatorial Pacific. Mar. Ecol. Prog. Ser. 652,
- 934 15–32.
- Landry, M.R., Swalethorp, R., 2021. Mesozooplankton biomass, grazing and trophic structure in the
- bluefin tuna spawning area of the oceanic Gulf of Mexico. J. Plankton Res.,
- 937 doi.10.1093/plankt/fbab008.
- Lee, S.-K., Park, W., Baringer, M.O., Gordon, A., Huber, B., Liu, Y., 2015. Pacific origin of the
- abrupt increase in Indian Ocean heat content during the warming hiatus. Nature Geosci. 8, 445–
- 940 450.
- Legand, M., 1969. Seasonal variations in the Indian Ocean along 110°E. VI. Macroplankton and
- micronekton biomass. Aust. J. Mar. Freshwater Res. 20, 85–103.
- Lessard, E.J., Murrell, M.C., 1998. Microzooplankton herbivory and phytoplankton growth in the
- northwestern Sargasso Sea. Aguat. Microb. Ecol. 16, 173–188.
- Lourey, M.J., Thompson, P.A., McLaughlin, M.J., Bonham, P., Feng, M., 2013. Primary production
- and phytoplankton community structure during a winter shelf-scale phytoplankton bloom off
- 947 Western Australia. Mar. Biol. 160, 355-369.
- Liu, H, Campbell, L., Landry, M.R., Nolla, H.A., Brown, S.L., Constantinou, J., 1998.
- *Prochlorococcus* and *Synechococcus* growth rates and contributions to production in the Arabian
- Sea during the 1995 Southwest and Northeast Monsoons. Deep-Sea Res. II 45, 2327–2352.
- Lund, J.W.G., Kipling, C., Le Cren, E.D., 1958. The inverted microscope method of estimating algal
- numbers and the statistical basis of estimations by counting. Hydrobiol. 11, 143–170.

- Mackas, D., Bohrer, R., 1976. Fluorescence analysis of zooplankton gut contents and an
- investigation of diel feeding patterns. J. Exp. Mar. Biol. Ecol. 25, 77-85.
- 955 Marra, J., Heinemann, K.R., 1987. Primary production in the North Pacific Central Gyre: some new
- measurements based on <sup>14</sup>C. Deep-Sea Res. 34, 1821–1829.
- 957 Menden-Deuer, S., Lessard, E.J., 2000. Carbon to volume relationships for dinoflagellates, diatoms,
- and other protist plankton. Limnol. Oceanogr. 45, 569–679.
- 959 McWilliam, P.S., 1977. Further studies of plankton ecosystems in the eastern Indian Ocean. VI.
- Ecology of the Euphausiacea. Aust. J. Mar. Freshwater Res. 28, 627–644.
- 961 Moore, L.R., 1997. Physiological ecology of *Prochlorococcus*: A Comparison of isolates from
- diverse oceanic regimes. Ph.D. Thesis. Dept. Civil and Environ. Engineering. Mass. Inst.
- 963 Technol.
- Monger, B.C., Landry, M.R., 1993. Flow cytometric analysis of marine bacteria with Hoechst
- 965 33342. Appl. Environ. Microbiol. 59, 905–911.
- Moriarty, R., O'Brien, T., 2013. Distribution of mesozooplankton biomass in the global ocean: Earth
- 967 Syst. Sci. Data 5, 45–55.
- Newell, B.S., 1969. Seasonal variations in the Indian Ocean along 110°E. II. Particulate carbon.
- 969 Aust. J. Mar. Freshwater Res. 20, 51–54.
- Paterson, H.L., Knott, B., Waite, A.M., 2007. Microzooplankton community structure and grazing
- on phytoplankton, in an eddy pair in the Indian Ocean off Western Australia. Deep-Sea Res. II
- 972 54, 1076–1093.
- Paterson, H.L., Knott, B., Koslow, A.J., Waite, A.M., 2008. The grazing impact of
- microzooplankton off south west Western Australia: as measured by the dilution technique. J.
- 975 Plankton Res. 30, 379–392.
- 976 Pfannkuche, O., Lochte, K., 1993. Open ocean pelago-benthic coupling: cyanobacteria as tracers of
- 977 sedimenting salp faeces. Deep-Sea Res I 40, 727–737.
- Pomroy, A., Joint, I. 1999. Bacterioplankton activity in the surface waters of the Arabian Sea during
- and after the 1994 SW monsoon. Deep-Sea Res. II 46, 767–794.
- Putt, M., Stoecker, D.K., 1989. An experimentally determined carbon: volume ratio for marine
- "oligotrichous" ciliates from estuarine and coastal waters. Limnol. Oceanogr. 34, 1097–1103

- Ras, J., Claustre, H., Uitz, J., 2008. Spatial variability of phytoplankton pigment distributions in the
- subtropical south Pacific Ocean: comparison between in situ and predicted data. Biogeosciences
- 984 5, 353–369.
- Rees, C., Pender, L., Sherrin, K., Schwanger, C., Hughes, P., Tibben, S., Marouchos, A., Rayner,
- 986 M., 2018. Methods for reproducible shipboard SFA nutrient measurement using RMNS and
- automated data processing. Limnol. Oceanogr. Methods 17, 5–41.
- Rochford, D.J., 1963. Some features of organic phosphorus distribution in the south-east Indian and
- south-west Pacific Oceans. Aust. J. Mar. Freshwater Res. 14, 119–138.
- 990 Rochford D.J., 1969. Seasonal variation in the Indian Ocean along 110°E. I. Hydrological structure
- of the upper 500 m. Aust. J. Mar. Freshwater Res. 20, 1–50.
- Rochford, D.J., 1977. Further studies of plankton ecosystems in the eastern Indian Ocean. II.
- Seasonal variations in water mass distribution (upper 150 m) along 110°E. (August 1962-August
- 994 1963). Aust. J. Mar. Freshwater Res. 28, 541–555.
- Roman, M., S. Smith, S., Wishner, K., Zhang, X.S., Gowing, M., 2000. Mesozooplankton
- production and grazing in the Arabian Sea. Deep Sea Res. II 47, 1423–1450.
- 997 Rossi, V., Feng, M., Pattiaratchi, C., Roughan, M., Waite, A.M., 2003. On the factors influencing the
- development of sporadic upwelling in the Leeuwin Current system. J. Geophys. Res. Oceans
- 999 118, 3608–3621.
- Sakthivel, M. 1977. Further studies of plankton ecosystems in the eastern Indian Ocean. VIII.
- seasonal, diurnal, and latitudinal variations in abundance of Euthecosomata along the 110°E.
- meridian. Aust. J. Mar. Freshwater Res. 28, 663–671.
- Säwström, C., Beckley, L.E., Saunders, M.I., Thompson, P.A., Waite, A.M., 2014. The zooplankton
- prey field for rock lobster phyllosoma larvae in relation to oceanographic features of the south-
- eastern Indian Ocean. J. Plankton Res. 36, 1–14.
- 1006 Selph, K.E., 2021b. Enumeration of marine microbial organisms by flow cytometry using near-UV
- excitation of Hoechst 34580-stained DNA. Limnol. Oceanogr. Methods, in press.
- 1008 Selph, K.E., Landry, M.R., Taylor, A.G., Gutiérrez-Rodríguez, A., Stukel, M.R., Wokuluk, J.,
- Pasulka, A.L., 2016. Phytoplankton production and taxon-specific growth rates in the Costa Rica
- 1010 Dome. J. Plankton Res. 38, 199–215.

- 1011 Selph, K.E., Landry, M.R., Taylor, A.G., Yang, E.J., Measures, C.I., Yang, J.J., Stukel, M.R.,
- 1012 Christensen, S., Bidigare, R.R., 2011. Spatially-resolved taxon-specific phytoplankton
- production and grazing dynamics in relation to iron distributions in the Equatorial Pacific
- 1014 between 110 and 140°W. Deep-Sea Res. II 58, 358–377.
- 1015 Selph, K.E., Swalethorp, R., Stukel, M.R., Kelly, T.B., Knapp, A. N., Fleming, K., Hernandez, T.,
- Landry, M.R., 2021a. Phytoplankton community composition and biomass in the oligotrophic
- Gulf of Mexico. J. Plankton Res., doi.10.1093/plankt/fbab006.
- Scheinberg, R.D., Landry, M.R., Calbet, A., 2005. Grazing of two common appendicularians on the
- natural prey assemblage of a tropical coastal ecosystem. Mar. Ecol. Prog. Ser. 294, 201–212.
- Shalapyonok, A., Olson, R.J., Shalapyonok, L.S., 2000. Arabian sea phytoplankton during the
- Southwest and Northeast Monsoons 1995: composition, size structure, and biomass from
- individual cell properties measured by flow cytometry. Deep-Sea Res. II 48, 1231–1261.
- Strickland, J.D.H., Parsons, T.R., 1972. A Practical Handbook of Seawater Analysis. Fisheries
- Research Board, Canada Ottawa.
- Strzelecki, J., Koslow, J.A., Waite, A.M., 2007. Comparison of mesozooplankton communities from
- a pair of warm- and cold-core eddies off the coast of Western Australia. Deep-Sea Res. II, 54,
- 1027 1103–1112.
- Stukel, M.R., Décima, M., Selph, K.E., Taniguchi, D.A., Landry, M.R., 2013. The role of
- 1029 Synechococcus in vertical flux in the Costa Rica upwelling dome. Prog. Oceanogr. 112, 49–59.
- Stukel, M.R., Landry, M.R. and Selph, K.E., 2011. Nanoplankton mixotrophy in the eastern
- equatorial Pacific. Deep-Sea Res. II 58, 378–386.
- Sutton, A.L., Beckley, L.E., 2016. Influence of the Leeuwin Current on the epipelagic euphausiid
- assemblages of the south-east Indian Ocean. Hydrobiol. 779, 193-207.
- 1034 Sverdrup, H.U., 1953. On conditions for the vernal blooming of phytoplankton. J. Cons. Internat.
- 1035 Explor. Mer 18, 287–295.
- Talley, L.D., 1995. Preliminary results from a WHP section in the Central Indian Ocean. Internat.
- 1037 WOCE Newslett. 21, 35–38.
- Taylor, A.G., Landry, M.R., Freibott, A., Selph, K.E., Gutiérrez-Rodríguez, A., 2016. Patterns of
- microbial community biomass, composition and HPLC diagnostic pigments in the Costa Rica
- upwelling dome. J. Plankton Res. 38, 183–198.

- Taylor, A.G., Landry, M.R., Selph, K.E., Yang, E.J., 2011. Biomass, size structure and depth
- distributions of the microbial community in the eastern equatorial Pacific. Deep-Sea Res. II 58,
- 1043 342–357.
- Taylor, A.H., Geider R.J., Gilbert, F.J.H., 1997. Seasonal and latitudinal dependencies of
- phytoplankton carbon-to-chlorophyll a ratios: results of a modelling study. Mar. Ecol. Prog. Ser.
- 1046 152, 51–66.
- Thompson, P.A., Wild-Allen, K., Lourey, M., Rousseaux, C., Waite, A.M., Feng, M., Beckley, L.E.
- 1048 2011. Nutrients in an oligotrophic boundary current: Evidence of a new role for the Leeuwin
- 1049 Current. Prog. Oceanogr. 91, 345-359.
- 1050 Tranter, D.J., 1977a. Further studies of plankton ecosystems in the eastern Indian Ocean. V. Ecology
- of the Copepoda. Aust. J. Mar. Freshwater Res. 28, 593–625.
- 1052 Tranter, H.A., 1977b. Further studies of plankton ecosystems in the eastern Indian Ocean. VII. The
- Ecology of the Amphipoda. Aust. J. Mar. Freshwater Res. 28, 645–642.
- 1054 Tranter, D.J., Kerr, J.D., 1969. Seasonal variation in the Indian Ocean along 110°E. V. Zooplankton
- biomass. Aust. J. Mar. Freshwater Res. 20, 77–84.
- 1056 Tranter, D.J., Kerr, J.D., 1977. Further studies of plankton ecosystems in the eastern Indian Ocean.
- III. Numerical abundance and biomass. Aust. J. Mar. Freshwater Res. 28, 557–583,
- Valencia, B., Décima, M., Landry, M.R., 2018. Environmental effects on mesozooplankton size
- structure and export flux at station ALOHA, North Pacific subtropical gyre. Glob. Biogeochem.
- 1060 Cyc. 32, 289–305.
- Valencia, B., Stukel, M.R., Allen, A.E., McCrow, J.P., Rabines, A., Palenik, B., Landry, M.R., 2021.
- Relating sinking and suspended microbial communities in the California Current Ecosystem:
- Digestion resistance and the contributions of phytoplankton taxa to export. Environ. Microbiol.
- 1064 doi:10.1111/1462-2920.15736.
- Vaulot, D., 1992. Estimate of phytoplankton division rates by the mitotic index method: The  $f_{max}$
- approach revisited. Limnol. Oceanogr. 37, 644–649.
- Vaulot, D., Marie, D., Olson, R.J., Chisholm, S.W., 1995. Growth of *Prochlorococcus*, a
- photosynthetic prokaryote, in the Equatorial Pacific Ocean. Science 268, 1480–1482.
- Veldhuis, M., Kraay, G., 2004. Phytoplankton in the subtropical Atlantic Ocean: towards a better
- assessment of biomass and composition. Deep-Sea Res. I 51, 507–530.

- Waite, A.M., Muhling, B.A., Holl, C.M., Beckley, L.E., Montoya, J.P., Strzeleckie, J., Thompson,
- 1072 P.A., Pesant, S., 2007b. Food web structure in two counter-rotating eddies based on  $\delta^{15}$ N and
- $\delta^{13}$ C isotopic analyses. Deep-Sea Res. II 54, 1055–1075.
- Waite, A.M., Pesant, S., Griffin, D.A., Thompson, P.A., Holl, C.M., 2007a. Oceanography, primary
- production and dissolved inorganic nitrogen uptake in two Leeuwin Current eddies. Deep-Sea
- 1076 Res. II 54, 981–1002.
- Waite, A.M., Raes, E., Beckley, L.E., Thompson, P.A., Griffin, D., Saunders, M., Säwström, C.,
- O'Rorke, R., Wang, M., Landrum, J.P., Jeffs, A., 2019. Production and ecosystem structure in
- 1079 cold-core vs. warm-core eddies: Implications for the zooplankton isoscape and rock lobster
- larvae. Limnol. Oceanogr. 64, 2405–2423.
- Wang, M., O'Rorke, R., Waite, A.M., Beckley, L.E., Thompson, P., Jeffs, A.G., 2014. Fatty acid
- profiles of phyllosoma larvae of western rock lobster (*Panulirus cygnus*) in cyclonic and
- anticyclonic eddies of the Leeuwin Current off Western Australia. Prog. Oceanogr. 122, 153–
- 1084 162.
- Waterbury, J.B., Watson, S.W., Guillard, R.R.L., Brand, L.E., 1979. Wide-spread occurrence of a
- unicellular, marine planktonic, cyanobacterium. Nature 277, 293–294.
- Wilson, S.E., Steinberg, D.K., 2010. Autotrophic picoplankton in mesozooplankton guts: evidence
- of aggregate feeding in the mesopelagic zone and export of small phytoplankton. Mar. Ecol.
- 1089 Prog. Ser. 412, 11–27.
- 1090 Woo, M., Pattiaratchi, C., 2008. Hydrography and water masses off the western Australian coast.
- 1091 Deep-Sea Res. I 55, 1090–1104.
- Worden, A., Nolan, J., Palenik, B., 2004. Assessing the dynamics and ecology of marine
- picophytoplankton: the importance of the eukaryotic component. Limnol. Oceanogr. 49, 168–
- 1094 179.
- 1095 Wyrtki, K., 1962. The upwelling in the region between Java and Australia during the south-east
- monsoon. Aust. J. Mar. Freshwater Res. 13, 217–225.
- Wyrtki, K., 1964. Upwelling in the Costa Rica dome. Fish. Bull. 63, 355–372.
- 1098 Yingling, N., Kelly, T.B., Selph, K.E., Landry, M.R., Knapp, A.N., Kranz S.A., Stukel, M.R., 2021.
- Taxon-specific phytoplankton growth, nutrient limitation, and light limitation in the oligotrophic
- Gulf of Mexico. J. Plankton Res., doi:10.1093/plankt/fbab028.

Zubkov, M., Sleigh, M., Burkill, P.H., Laekey, R., 2000. Picoplankton community structure on the
 Atlantic Meridonal Transect: a comparison between seasons. Prog. Oceanog. 45, 369–386.
 1103

## 1104 Figure legends

1124

1125

1126

1127

1128

1129

- 1105 Fig. 1. Station locations and environmental parameter sections from CTD profiles conducted 1106 along 110°E. Indonesia is north of 10°S and Australia is to the east in station map (a). 1107 Temperature (b), salinity (c) and Chla fluorescence (e) are from continuous CTD 1108 instrument measurements averaged at 1-m depth intervals. Nitrate+Nitrite 1109 concentrations (d) are from shipboard analyses at discrete sampling depths. Black line 1110 in Panel d is Mixed Layer Depth (MLD), defined as the depth at which temperature 1111 decreases 0.1 °C below surface values (Landry et al., 2020). White line in Panel e is the 1112 Euphotic Zone (EZ), the depth of penetration of 1% of surface irradiance calculated 1113 from the mean coefficient of light extinction (PAR) (Landry et al., 2020).
- Fig. 2. Station profiles of Temperature (°C), Nitrate+Nitrite concentration (μM) and extracted

  Chla (mg m<sup>-3</sup>) from the CTD water samples collected at six light depths (% I₀) along

  110°E. Station locations (Latitude, °S) are indicated in the color-coded legend.
- Fig. 3. Relationships between bead-normalized red fluorescence from flow cytometry and measured values of chlorophyll *a* from high-pressure liquid chromatography (HPLC).

  Data are all euphotic zone samples collected on evening CTD hydrocasts on the 110°E transect. a) Population red fluorescence for *Prochlorococcus* (PRO, cell abundance x mean cell fluorescence) relative to divinyl Chl*a* (DVChl*a*, μg L<sup>-1</sup>). b) Total red fluorescence for *Prochlorococcus*, *Synechococcus* and photosynthetic eukaryotes (sum of population abundances x mean cell fluorescence) relative to Total Chl*a* (TChl*a*, μg L<sup>-1</sup>).
  - **Fig. 4.** Euphotic-zone (EZ) integrated estimates of chlorophyll *a* contained in *Prochlorococcus* (PRO), *Synechococcus* (SYN) and photosynthetic eukaryotes (EUK) along the 110°E transect. a) Chl*a* concentrations (mg m<sup>-2</sup>) based on flow cytometric measurements of bead-normalized red fluorescence. b) Percent contributions (%) of population Chl*a* based on bead-normalized red fluorescence. c) Percent of Chl*a* explained by total red fluorescence relative to EZ-integrated Chl*a* from HPLC (TChl) and fluorometric (FlChl) analyses.

1134		°S) are indicated in the color-coded legend. Profiles exclude data from one sample at
1135		18% I <sub>0</sub> at 38°S for which all populations were anomalously low by a factor of 2,
1136		suggesting either a premature bottle trip or machine measurement error.
1137	Fig. 6.	Carbon:chlorophyll (C:Chla) profiles for flow cytometry populations at sampled light
1138		depths (% $I_o$ ) along the 110°E transect. PRO = Prochlorococcus; SYN =
1139		Synechococcus; EUK = photosynthetic eukaryotes; All FCM = combined PRO, SYN
1140		and EUK populations. Station locations (Latitude, °S) are indicated in the color-coded
1141		legend. Profiles exclude data from one sample at $18\%~I_0$ at $38^\circ S$ for which all
1142		populations were anomalously low by a factor of 2.
1143	Fig. 7.	Euphotic-zone integrated estimates of carbon biomass for Prochlorococcus (PRO),
1144		Synechococcus (SYN) and photosynthetic eukaryotes (EUK) along the 110°E transect.
1145		a) Carbon biomass (mg C m <sup>-2</sup> ) based on flow cytometric measurements of population
1146		abundances and mean cell carbon contents. b) Percent Contributions (%) of populations
1147		to total carbon biomass.
1148	Fig. 8.	Euphotic-zone (EZ) integrated estimates of carbon biomass for heterotrophic bacteria
1149		(HBAC), dinoflagellates (DINO), ciliates (CILIATE) and mesozooplankton (MESO)
1150		along the 110°E transect. a) HBAC biomass is based on flow cytometric measurements
1151		of population abundances and mean cell carbon. b) DINO and CILIATE biomass based
1152		on microscopical estimates for the upper EZ extrapolated to the full EZ. c) MESO
1153		biomass is based on average measured C biomass in day and night net tows.
1154	Fig. 9.	Growth rates and microzooplankton grazing mortality for flow cytometry populations
1155		from dilution experiments incubated at euphotic-zone light depths (% $I_{\text{o}}$ ) along the
1156		110°E transect. PRO = Prochlorococcus; SYN = Synechococcus; EUK =
1157		$photosynthetic\ eukaryotes;\ HBAC=heterotrophic\ bacteria.\ Station\ locations\ (Latitude,$
1158		°S) are indicated in the color-coded legend.
1159	Fig. 10.	. Chlorophyll-based growth rates (a) and microzooplankton grazing (b) from dilution
1160		experiments incubated at euphotic-zone light depths (% $I_o$ ) along the 110°E transect.
1161		Station locations (Latitude, °S) are indicated in color-coded legend.
1162	Fig. 11.	Integrated euphotic-zone (EZ) estimates of carbon production (PROD) and grazing
1163		(GRAZ) rates along the 110°E transect. a) PROD and microzooplankton grazing

(MICRO GRAZ) rates (mg C m<sup>-2</sup>) based on flow cytometric populations 1164 1165 Prochlorococcus (PRO), Synechococcus (SYN) and photosynthetic eukaryotes (EUK). 1166 b) PROD and MICRO GRAZ rates (mg C m<sup>-2</sup>) from dilution experiments based on Chla. MESO GRAZ based on the fraction of Chla removed by mesozooplankton d<sup>-1</sup> 1167 1168 and integrated values of C:Chla. c) PROD and MICRO GRAZ of heterotrophic bacteria 1169 (HBAC). 1170 Fig. 12. Relationships between euphotic-zone integrated estimates of phytoplankton production 1171 (PROD) and grazing (GRAZ) for phytoplankton and heterotrophic bacteria (HBAC) along the 110°E transect. a) Blue diamond (FCM) symbols are from combined flow 1172

along the 110°E transect. a) Blue diamond (FCM) symbols are from combined flow cytometry populations (PRO, SYN and EUK) from Figure 11a; red circles (CHL) are Chla from Figure 11b, and GRAZ is combined micro- and mesozooplankton grazing (MICRO+MESO) from Figure 11a,b. b) HBAC PROD and MICRO GRAZ from Fig.

1176 11c. All regressions are forced through zero.

1173

1174

1175

**Table 1**. Sample collection and incubation conditions for shipboard dilution experiments conducted along the 110°E transect in May-June 2019. Date is the day of sample collection and beginning of the 24-h incubation. Sampling conditions are wind speed (km h<sup>-1</sup>) and incident PAR (E m<sup>-2</sup> d<sup>-1</sup>) during the daytime period of the day of sample collection. Incubation onditions are PAR and mean seawater temperature in the running seawater line over the day of experimental incubation. Parameters were each measured by two instruments. Uncertainties are standard errors of mean values.

5 17 May 0 18 May 5 19 May 0 20 May 5 21 May 0 22 May 5 23 May 0 24 May 5 25 May	$30.9 \pm 0.2$ $45.0 \pm 0.4$ $40.7 \pm 0.1$ $25.8 \pm 0.1$ $12.6 \pm 0.1$ $18.2 \pm 0.2$ $27.7 \pm 0.2$	$13.2 \pm 0.2$ $9.8 \pm 0.2$ $5.3 \pm 0.1$ $20.4 \pm 0.1$ $15.2 \pm 0.1$ $18.7 \pm 0.1$ $16.8 \pm 0.4$ $19.0 \pm 0.5$	$9.8 \pm 0.2$ $5.3 \pm 0.1$ $20.4 \pm 0.1$ $15.2 \pm 0.1$ $18.7 \pm 0.1$ $16.8 \pm 0.4$ $19.0 \pm 0.5$ $17.7 \pm 0.4$	$18.06 \pm 0$ $18.12 \pm 0$ $19.16 \pm 0$ $20.26 \pm 0$
5 19 May 0 20 May 5 21 May 0 22 May 5 23 May 0 24 May	$45.0 \pm 0.4$ $40.7 \pm 0.1$ $25.8 \pm 0.1$ $12.6 \pm 0.1$ $18.2 \pm 0.2$ $27.7 \pm 0.2$	$5.3 \pm 0.1$ $20.4 \pm 0.1$ $15.2 \pm 0.1$ $18.7 \pm 0.1$ $16.8 \pm 0.4$	$20.4 \pm 0.1$ $15.2 \pm 0.1$ $18.7 \pm 0.1$ $16.8 \pm 0.4$ $19.0 \pm 0.5$	$15.33 \pm 0$ $18.06 \pm 0$ $18.12 \pm 0$ $19.16 \pm 0$ $20.26 \pm 0$ $20.69 \pm 0$
0 20 May 5 21 May 0 22 May 5 23 May 0 24 May	$40.7 \pm 0.1$ $25.8 \pm 0.1$ $12.6 \pm 0.1$ $18.2 \pm 0.2$ $27.7 \pm 0.2$	$20.4 \pm 0.1$ $15.2 \pm 0.1$ $18.7 \pm 0.1$ $16.8 \pm 0.4$	$15.2 \pm 0.1$ $18.7 \pm 0.1$ $16.8 \pm 0.4$ $19.0 \pm 0.5$	$18.12 \pm 0$ $19.16 \pm 0$ $20.26 \pm 0$
5 21 May 0 22 May 5 23 May 0 24 May	$25.8 \pm 0.1$ $12.6 \pm 0.1$ $18.2 \pm 0.2$ $27.7 \pm 0.2$	$15.2 \pm 0.1$ $18.7 \pm 0.1$ $16.8 \pm 0.4$	$18.7 \pm 0.1$ $16.8 \pm 0.4$ $19.0 \pm 0.5$	$19.16 \pm 0$ $20.26 \pm 0$
0 22 May 5 23 May 0 24 May	$12.6 \pm 0.1$ $18.2 \pm 0.2$ $27.7 \pm 0.2$	$18.7 \pm 0.1$ $16.8 \pm 0.4$	$16.8 \pm 0.4$ $19.0 \pm 0.5$	$20.26 \pm 0$
5 23 May 0 24 May	$18.2 \pm 0.2$ $27.7 \pm 0.2$	$16.8 \pm 0.4$	$19.0\pm0.5$	
0 24 May	$27.7 \pm 0.2$			$20.69 \pm 0$
,		$19.0\pm0.5$	$17.7 \pm 0.4$	
5 25 May			$1/./ \pm 0.4$	$21.85 \pm 0$
3	$36.2 \pm 0.1$	$17.7 \pm 0.4$	$28.4 \pm 1.9$	$23.31 \pm 0$
0 26 May	$36.2 \pm 0.3$	$28.4 \pm 1.9$	$25.8 \pm 1.1$	$24.06 \pm 0$
5 27 May	$7.8 \pm 0.0$	$25.8 \pm 1.1$	$27.6 \pm 0.9$	$24.88 \pm 0$
0 28 May	$12.7 \pm 0.3$	$27.6 \pm 0.9$	$34.4 \pm 1.8$	$25.58 \pm 0$
5 29 May	$19.4 \pm 0.3$	$34.4\pm1.8$	$34.3 \pm 2.4$	$26.44 \pm 0$
0 30 May	$19.2 \pm 0.4$	$34.3 \pm 2.4$	$37.4 \pm 0.8$	$26.88 \pm 0$
5 31 May	$29.2 \pm 0.1$	$37.4 \pm 0.8$	$37.3 \pm 0.8$	$27.10 \pm 0$
0 1 June	$40.7 \pm 0.1$	$37.3 \pm 0.8$	$35.7 \pm 1.6$	$27.31 \pm 0$
5 2 June	$36.5 \pm 0.0$	$35.7 \pm 1.6$	$35.8 \pm 1.0$	$28.01 \pm 0$
0 3 June	$31.2\pm0.1$	$35.8 \pm 1.0$	$36.0 \pm 0.9$	$28.07 \pm 0$
5 4 June	$24.9 \pm 0.1$	$36.0 \pm 0.9$	$37.6 \pm 3.4$	$28.11 \pm 0$
	$10.4 \pm 0.4$	$37.6 \pm 3.4$	$21.1 \pm 0.5$	$28.06 \pm 0$
(	0 1 June 5 2 June 0 3 June 5 4 June	0 1 June $40.7 \pm 0.1$ 5 2 June $36.5 \pm 0.0$ 0 3 June $31.2 \pm 0.1$	1 June $40.7 \pm 0.1$ $37.3 \pm 0.8$ 2 June $36.5 \pm 0.0$ $35.7 \pm 1.6$ 3 June $31.2 \pm 0.1$ $35.8 \pm 1.0$ 4 June $24.9 \pm 0.1$ $36.0 \pm 0.9$	0 1 June $40.7 \pm 0.1$ $37.3 \pm 0.8$ $35.7 \pm 1.6$ 5 2 June $36.5 \pm 0.0$ $35.7 \pm 1.6$ $35.8 \pm 1.0$ 0 3 June $31.2 \pm 0.1$ $35.8 \pm 1.0$ $36.0 \pm 0.9$ 5 4 June $24.9 \pm 0.1$ $36.0 \pm 0.9$ $37.6 \pm 3.4$

Table 2. Comparisons of biomass, production and grazing rates measured along 110°E in May1210 June 2019 to measurements from open-ocean studies in the Arabian Sea, Gulf of Mexico,
1211 equatorial Pacific and eastern tropical Pacific (Costa Rica Dome). ML = Mixed Layer; EZ =
1212 Euphotic Zone; TChla = Total chlorophyll a (HPLC). All measurements integrated to EZ depth
1213 defined by penetration of 1% Io.

1214
------

1215 1216	Variable	East IO 110°E¹	Arabian Sea <sup>2</sup>	Gulf of Mexico <sup>3</sup>	Equatorial Pacific <sup>4</sup>	East Trop Pacific <sup>5</sup>
1217	Profiles (n)	19	27	11	30	16
1218	Latitude	11.5-39.5 °S	10-23 °N	25-28 °N	4°S-4°N	6-11 °N
1219	ML Temp (°C)	12 - 28	20 - 29	24 - 27	24 - 27	26 - 29
1220	1% EZ Depth (m)	66 - 108	42 - 131	80 - 115	66 - 108	42 - 59
1221	TChla (mg m <sup>-2</sup> )	11 - 23	18 - 124	8 - 14	12 - 28	6 - 43
1222	Biomass (mg C m <sup>-2</sup> )					
1223	Phototrophs	967 - 1604	720 - 2890	849 - 1688	594 - 1766	828 - 2424
1224	H-Bacteria	391 - 616	510 - 1740	414 - 722	180 - 738	189 - 622
1225	Microzoo	18 - 379*	320 - 1350	146 - 724	233 - 870	145 - 479
1226	Mesozoo	131 - 488	360 - 5016	89 - 864	268 - 1580	580 - 6900
1227	Rate (mg C m <sup>-2</sup> d <sup>-1</sup> )					
1228	Phyto PROD	111 - 1201	600 - 2420	184 - 652	268 - 1426	291 - 1592
1229	Microzoo GRAZ	113 - 1131	258 - 1999	48 - 499	248 - 1091	148 - 923
1230	Mesozoo GRAZ	15 - 233	35 - 721	7 - 29	64 - 593	78 - 938

References: 1) this study, Landry et al. (2020a); 2) Landry et al. (1998), Caron and Dennett (1999), Garrison et al. (2000), Roman et al. (2000), Barber et al. (2001), Landry (2009); 3) Landry et al. (2021), Landry and Swalethorpe (2021), Selph et al. (2021), Yingling et al. (2021); 4) Balch et al. (2011), Décima et al. (2011), Landry et al. (2011), Selph et al. (2011), Taylor et al. (2011); 5) Décima et al. (2016), Freibott et al. (2016), Landry et al. (2016b), Selph et al. (2016), Taylor et al. (2016).

\*Microzooplankton biomass values for the present study are underestimated relative to others because they are missing contributions of non-plastidic flagellates from epifluorescence microscopy.

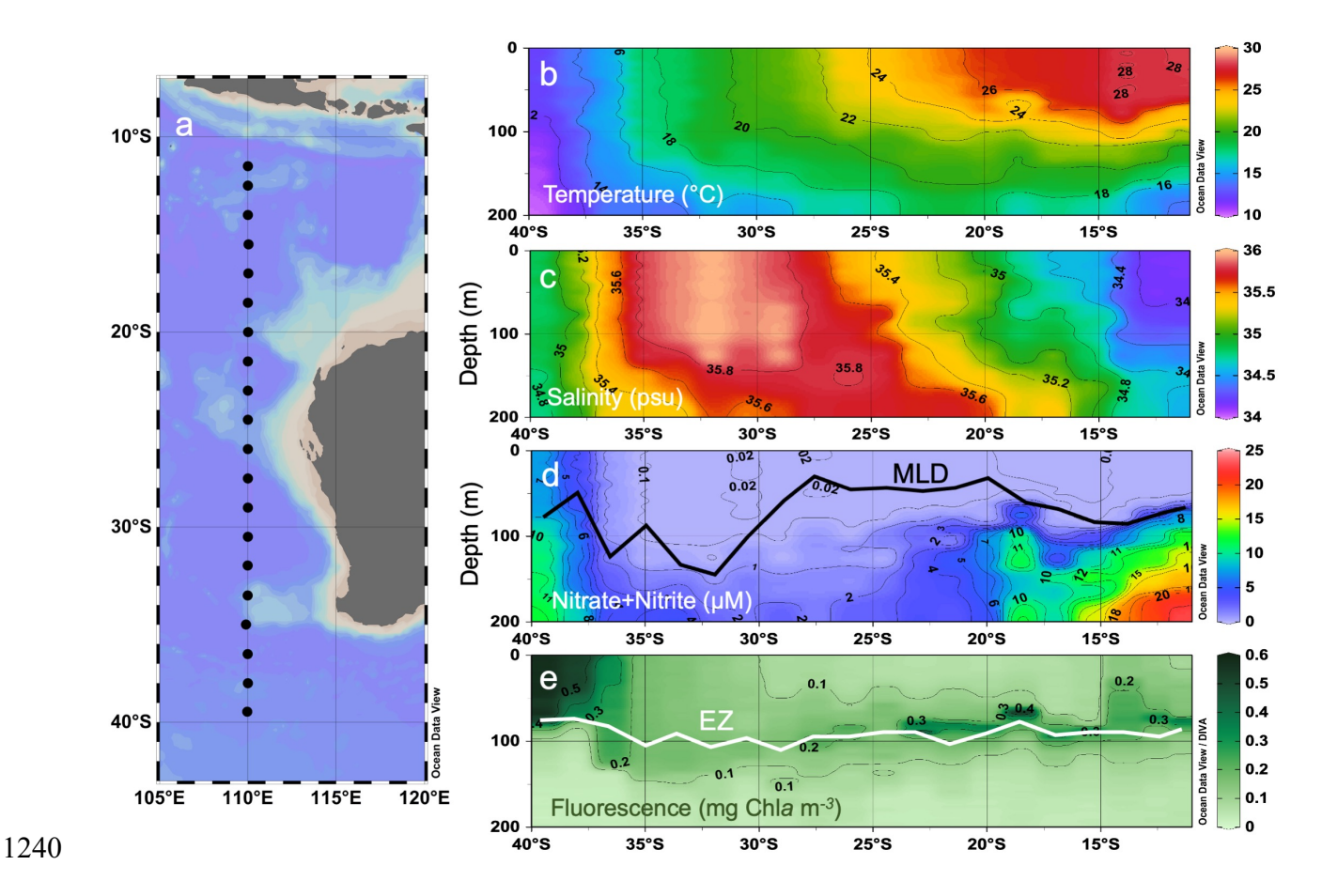
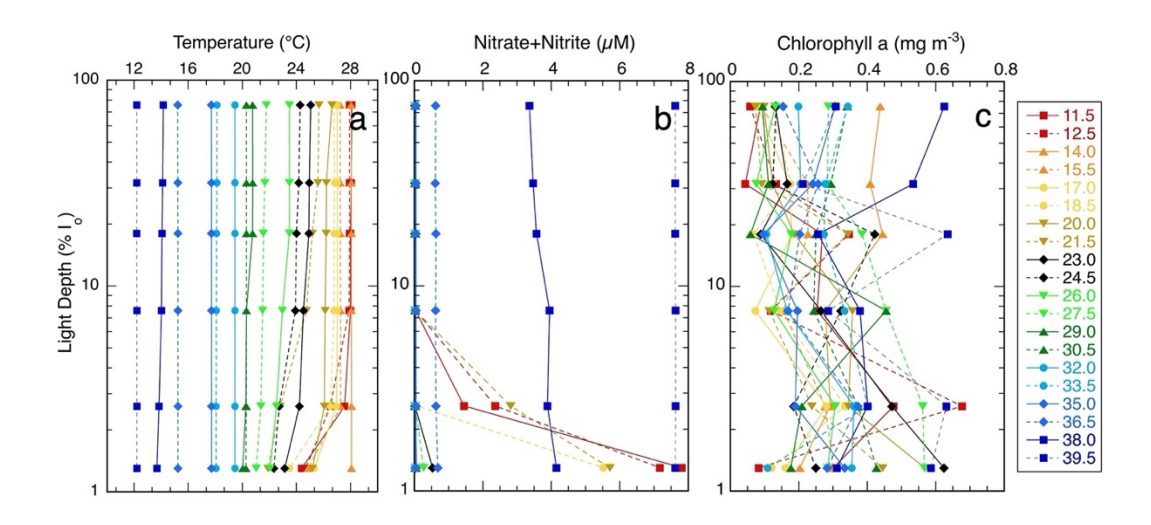
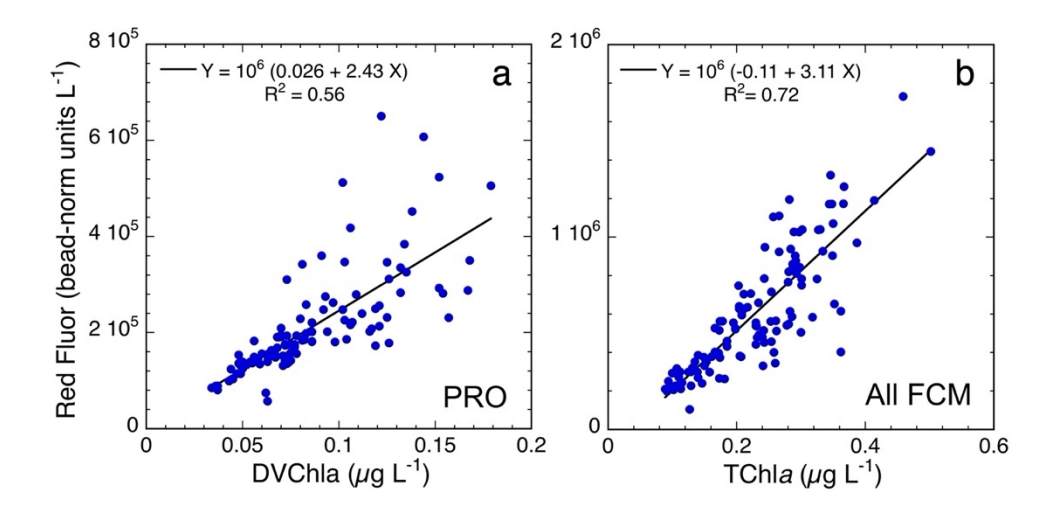


Fig. 1. Station locations and environmental parameter sections from CTD profiles conducted along 110°E. Indonesia is north of 10°S and Australia is to the east in station map (a). Temperature (b), salinity (c) and Chla fluorescence (e) are from continuous CTD instrument measurements averaged at 1-m depth intervals. Nitrate+Nitrite concentrations (d) are from shipboard analyses at discrete sampling depths. Black line in Panel d is Mixed Layer Depth (MLD), defined as the depth at which temperature decreases 0.1 °C below surface values (Landry et al., 2020). White line in Panel e is the Euphotic Zone (EZ), the depth of penetration of 1% of surface irradiance calculated from the mean coefficient of light extinction (PAR) (Landry et al., 2020).



**Fig. 2.** Station profiles of Temperature (°C), Nitrate+Nitrite concentration (μM) and extracted Chla (mg m<sup>-3</sup>) from the CTD water samples collected at six light depths (% I<sub>o</sub>) along 110°E. Station locations (Latitude, °S) are indicated in the color-coded legend.



**Fig. 3.** Relationships between bead-normalized red fluorescence from flow cytometry and measured values of chlorophyll *a* from high-pressure liquid chromatography (HPLC). Data are all euphotic zone samples collected on evening CTD hydrocasts on the 110°E transect. a) Population red fluorescence for *Prochlorococcus* (PRO, cell abundance x mean cell fluorescence) relative to divinyl Chl*a* (DVChl*a*, μg L<sup>-1</sup>). b) Total red fluorescence for *Prochlorococcus*, *Synechococcus* and photosynthetic eukaryotes (sum of population abundances x mean cell fluorescence) relative to Total Chl*a* (TChl*a*, μg L<sup>-1</sup>).

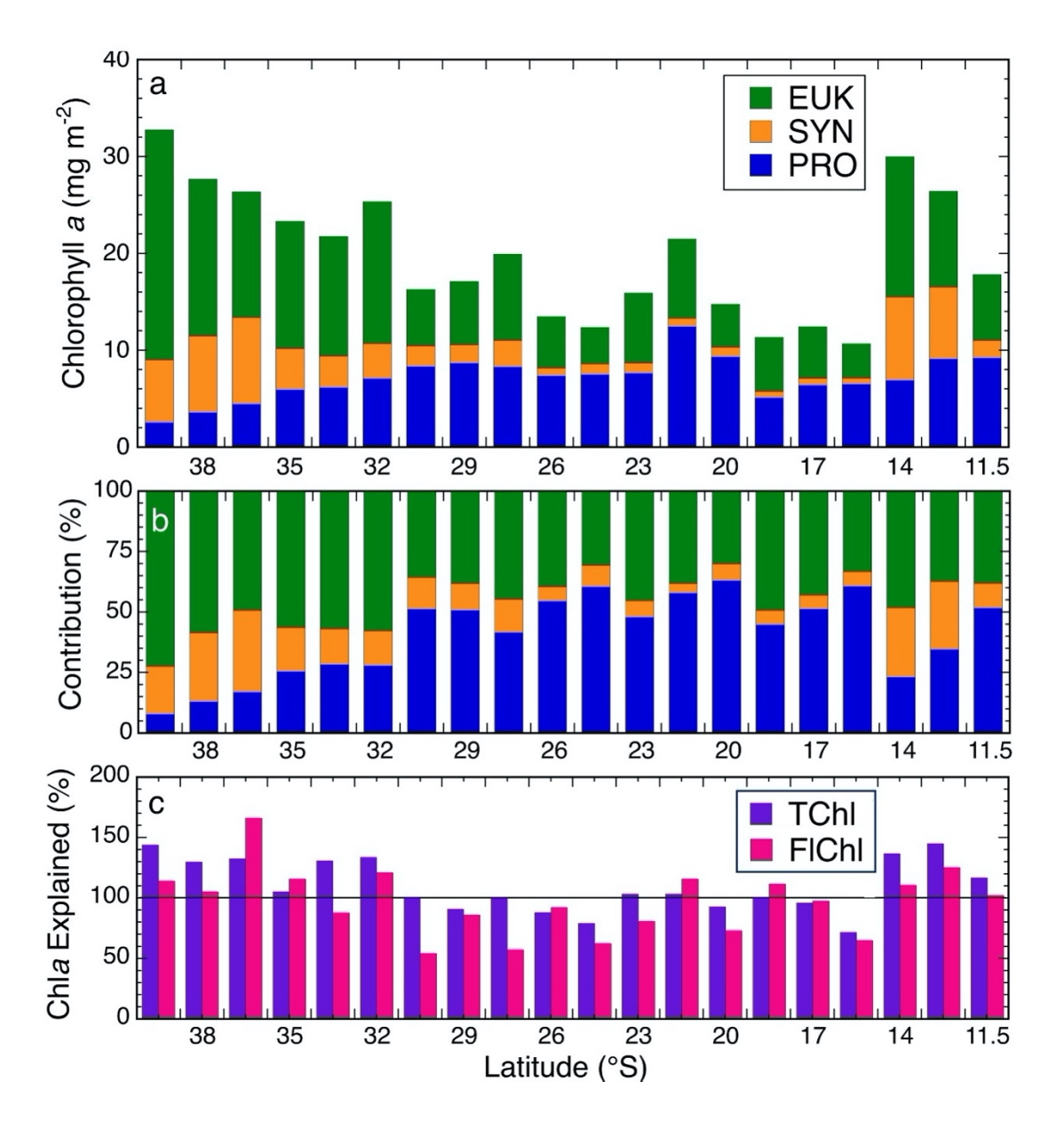


**Fig. 4.** Euphotic-zone (EZ) integrated estimates of chlorophyll *a* contained in *Prochlorococcus* (PRO), *Synechococcus* (SYN) and photosynthetic eukaryotes (EUK) along the 110°E transect. a) Chla concentrations (mg m<sup>-2</sup>) based on flow cytometric measurements of bead-normalized red fluorescence. b) Percent Contributions (%) of population Chla based on bead-normalized red fluorescence. c) Percent of Chla explained by total red fluorescence relative to EZ-integrated Chla from HPLC (TChl) and fluorometric (FlChl) analyses.

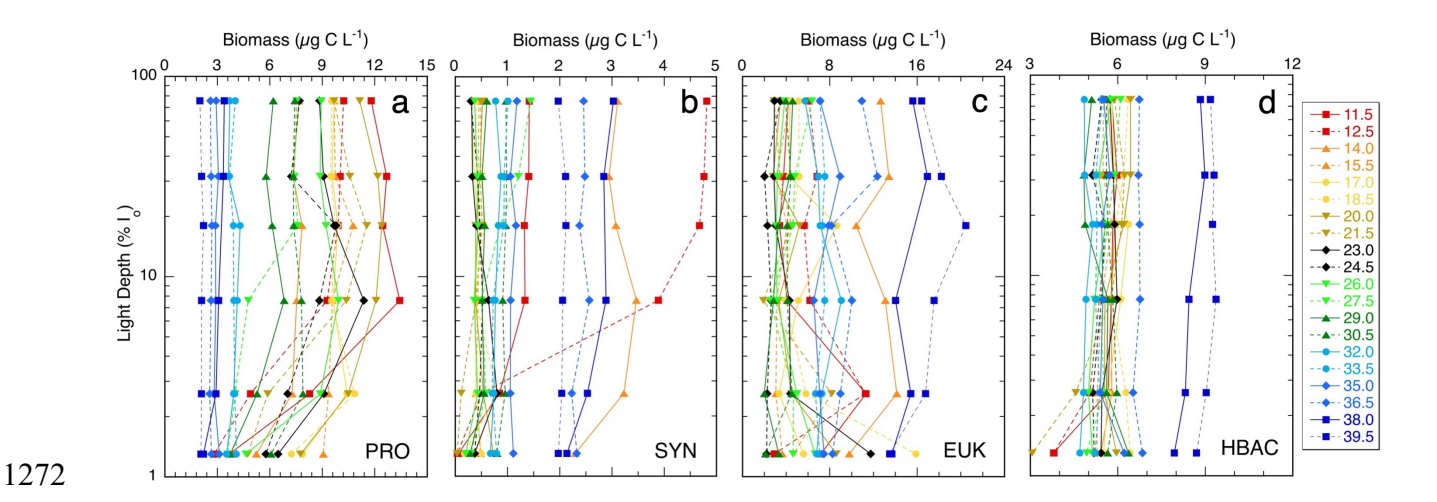


**Fig. 5.** Biomass profiles for flow cytometry populations at sampled light depths (% I<sub>o</sub>) along the 110°E transect. PRO = *Prochlorococcus*; SYN = *Synechococcus*; EUK = photosynthetic eukaryotes; HBAC = heterotrophic bacteria. Station locations (Latitude, °S) are indicated in the color-coded legend. Profiles exclude data from one sample at 18% I<sub>o</sub> at 38°S for which all populations were anomalously low by a factor of 2, suggesting either a premature bottle trip or machine measurement error.

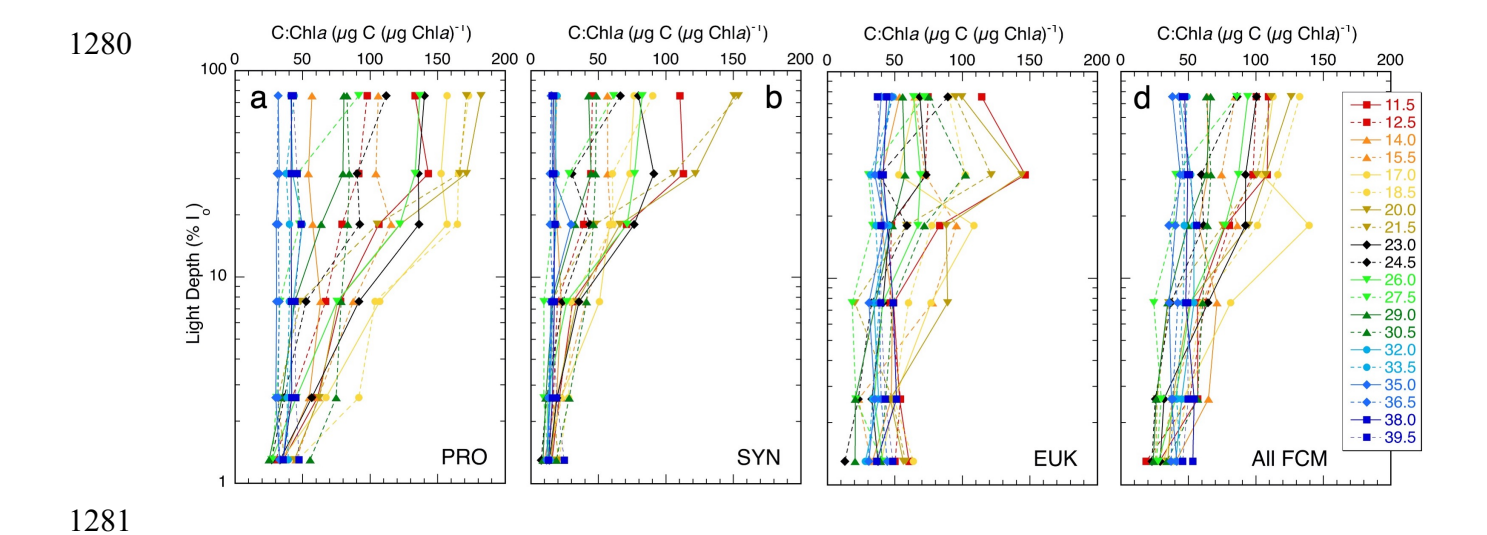


Fig. 6. Carbon:chlorophyll (C:Chla) profiles for flow cytometry populations at sampled light depths (% I<sub>0</sub>) along the 110°E transect. PRO = *Prochlorococcus*; SYN = *Synechococcus*; EUK = photosynthetic eukaryotes; All FCM = combined PRO, SYN and EUK 1285 populations. Station locations (Latitude, °S) are indicated in the color-coded legend. Profiles exclude data from one sample at 18% I<sub>0</sub> at 38°S for which all populations were anomalously low by a factor of 2.

1283

1284

1286

1287

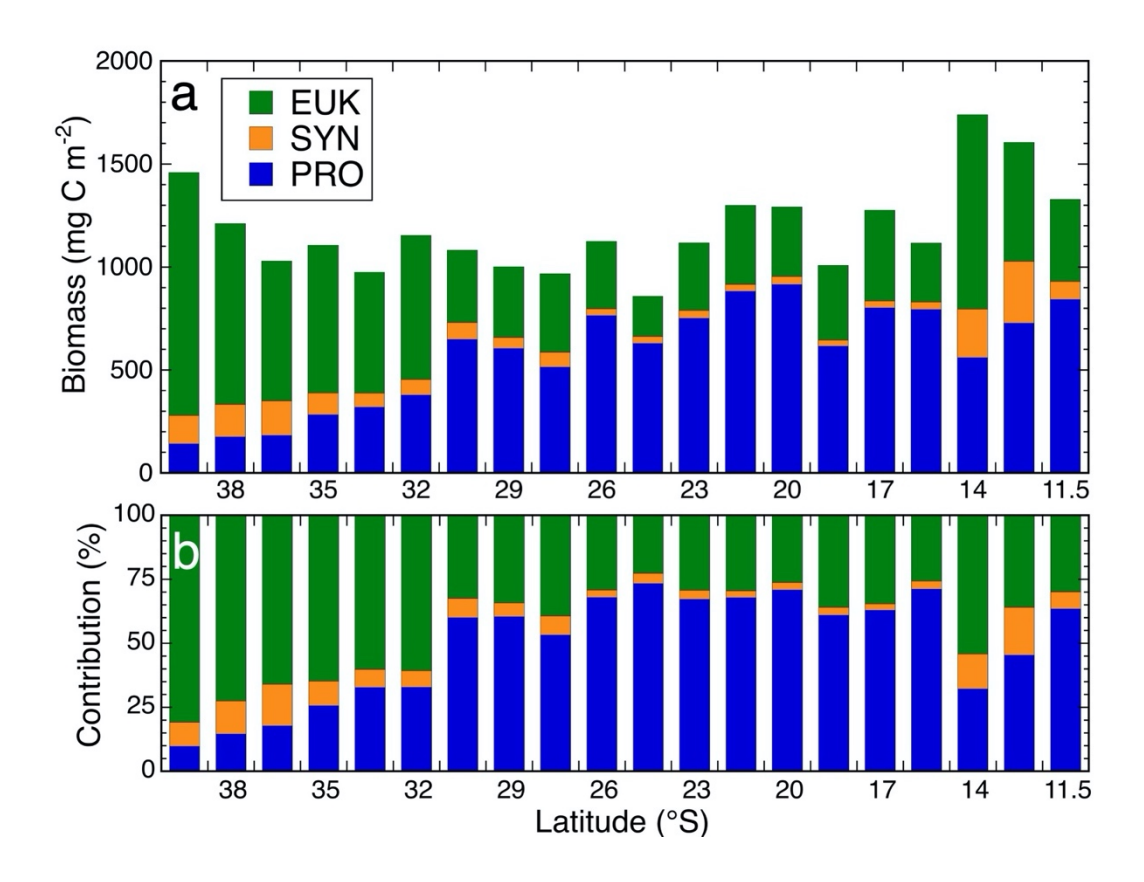


**Fig. 7.** Euphotic-zone integrated estimates of carbon biomass for *Prochlorococcus* (PRO), *Synechococcus* (SYN) and photosynthetic eukaryotes (EUK) along the 110°E transect. a) Carbon biomass (mg C m<sup>-2</sup>) based on flow cytometric measurements of population abundances and mean cell carbon contents. b) Percent Contributions (%) of populations to total carbon biomass.

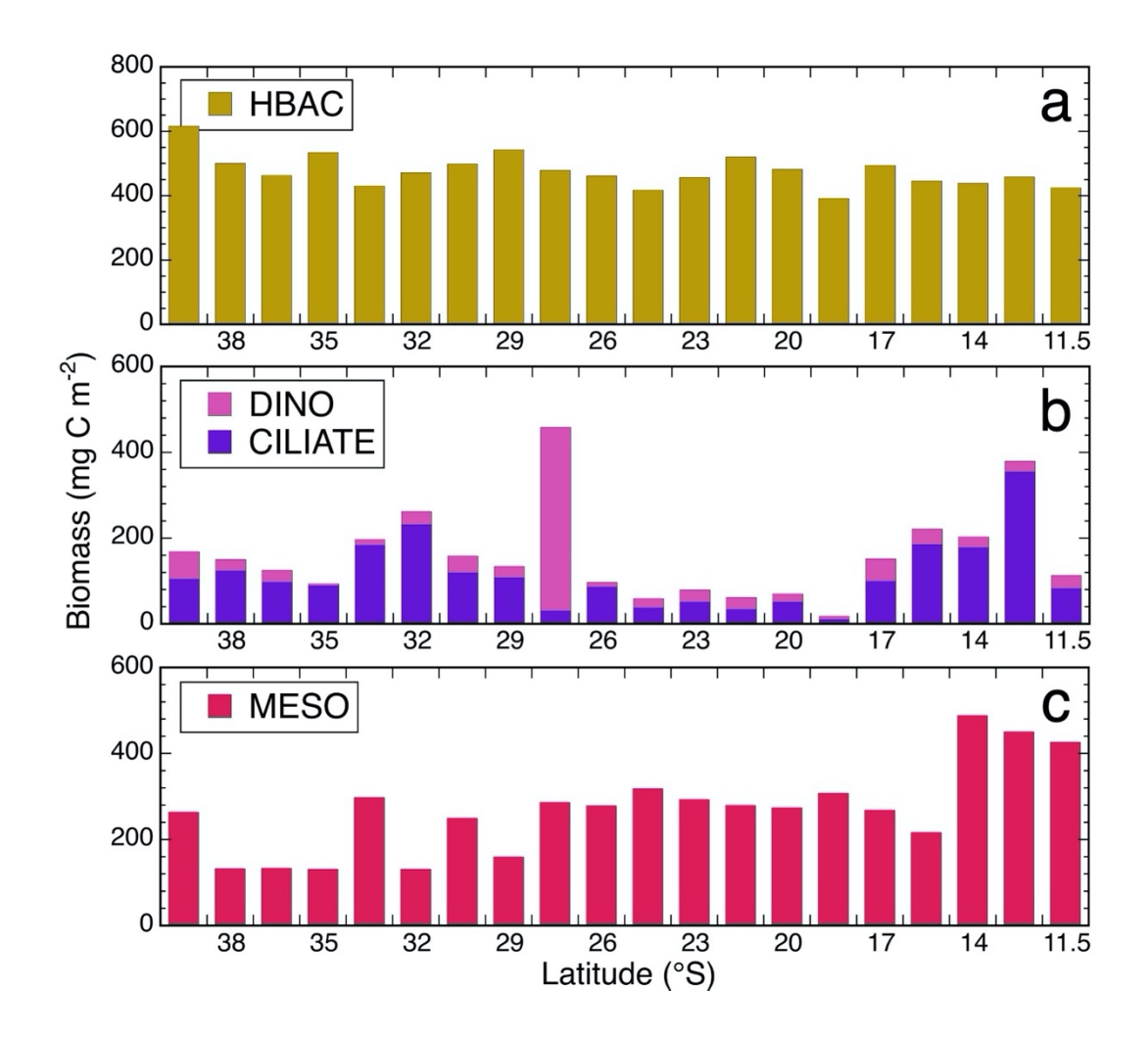


**Fig. 8.** Euphotic-zone (EZ) integrated estimates of carbon biomass for heterotrophic bacteria (HBAC), dinoflagellates (DINO), ciliates (CILIATE) and mesozooplankton (MESO) along the 110°E transect. a) HBAC biomass is based on flow cytometric measurements of population abundances and mean cell carbon. b) DINO and CILIATE biomass based on microscopical estimates for the upper EZ extrapolated to the full EZ. c) MESO biomass is based on average measured C biomass in day and night net tows.

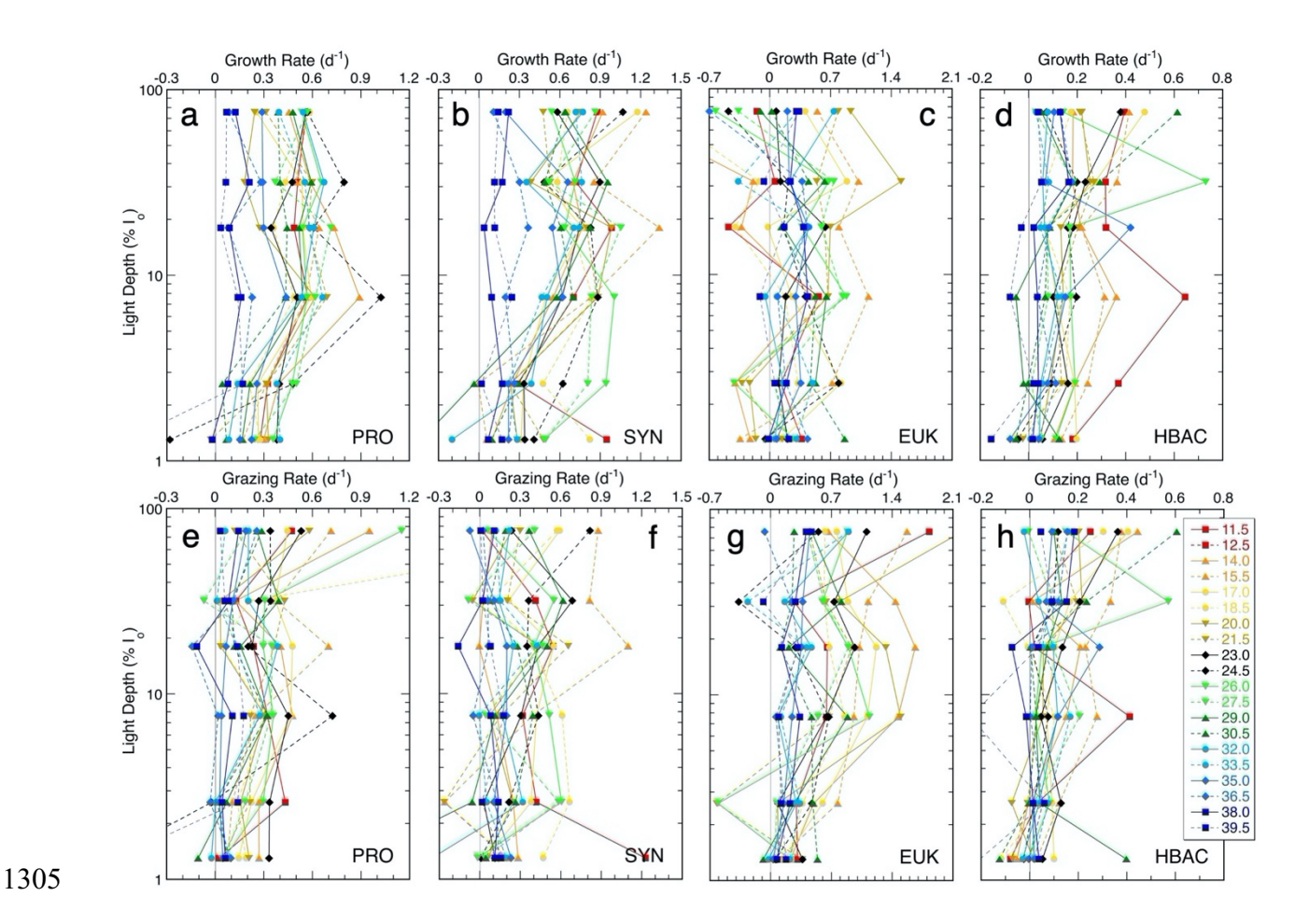


**Fig. 9.** Growth rates and microzooplankton grazing mortality for flow cytometry populations from dilution experiments incubated at euphotic-zone light depths (% I<sub>o</sub>) along the 110°E transect. PRO = *Prochlorococcus*; SYN = *Synechococcus*; EUK = photosynthetic eukaryotes; HBAC = heterotrophic bacteria. Station locations (Latitude, °S) are indicated in the color-coded legend.

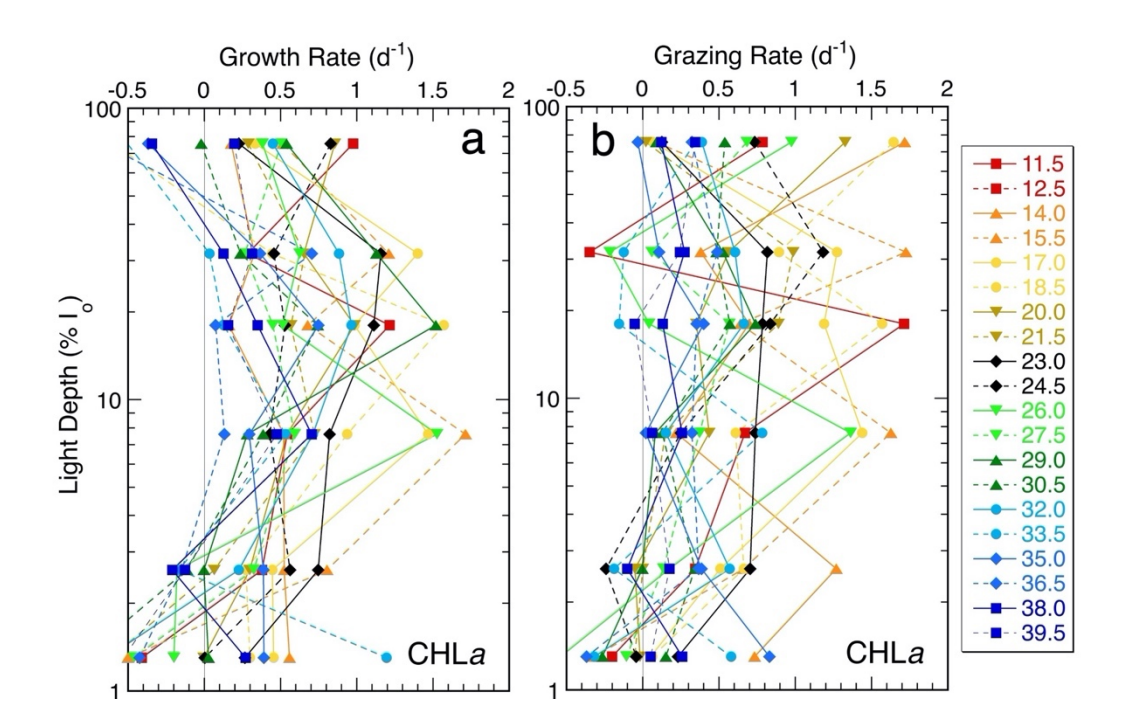
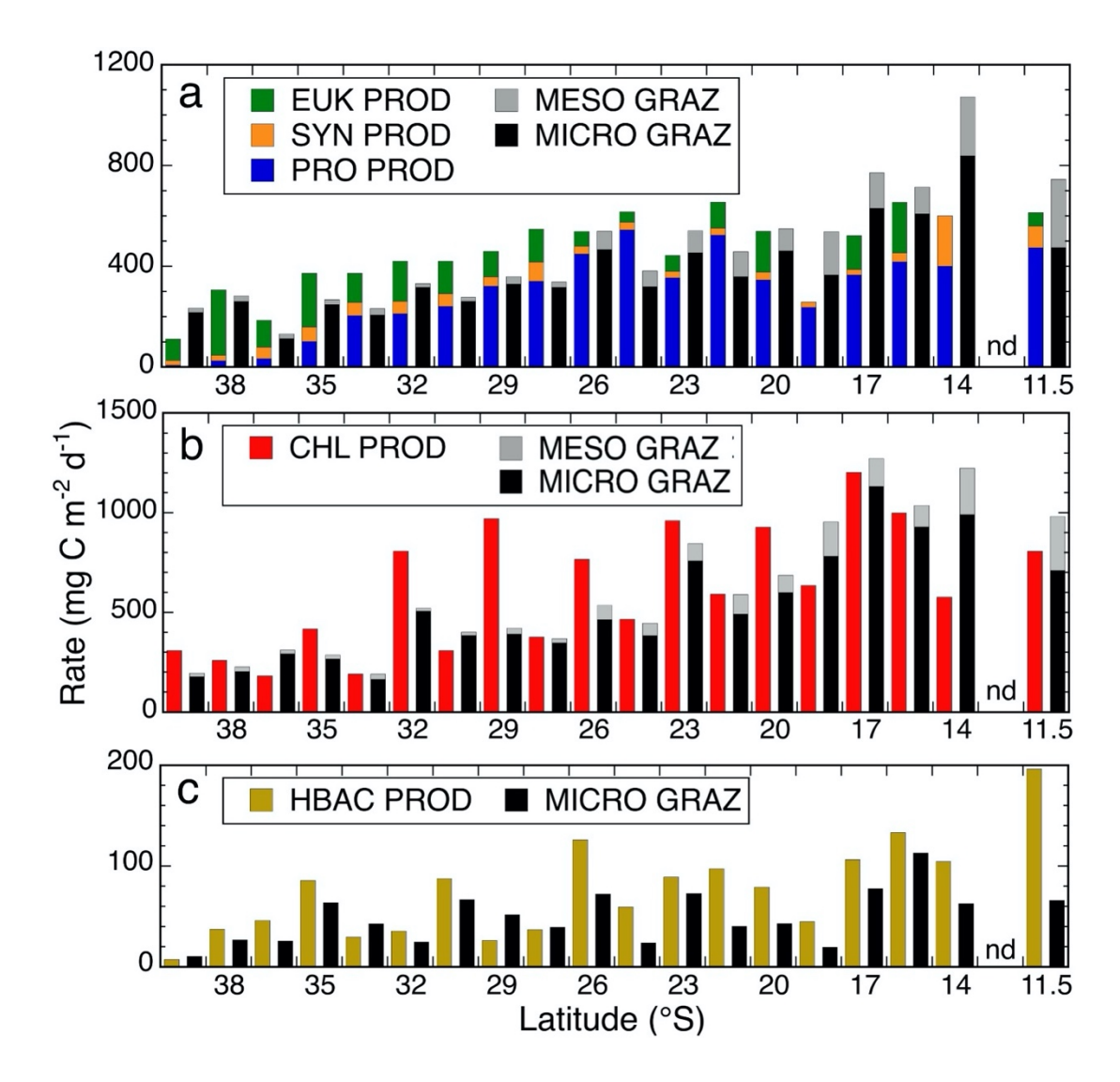
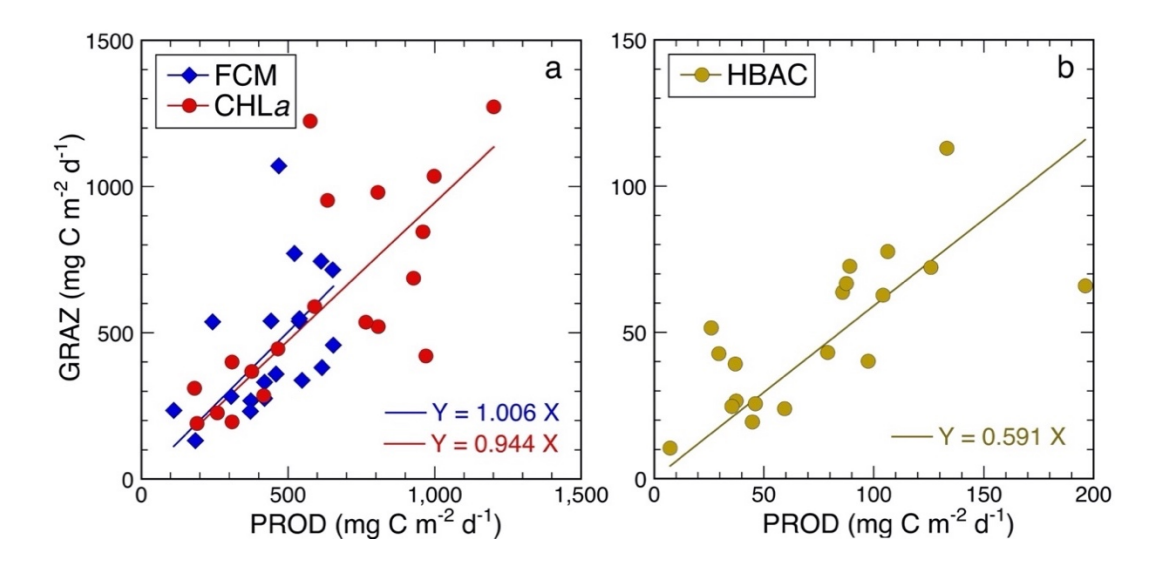


Fig. 10. Chlorophyll-based growth rates (a) and microzooplankton grazing (b) from dilution experiments incubated at euphotic-zone light depths (%  $I_o$ ) along the 110°E transect. Station locations (Latitude, °S) are indicated in color-coded legend.



**Fig. 11.** Integrated euphotic-zone (EZ) estimates of carbon production (PROD) and grazing (GRAZ) rates along the 110°E transect. a) PROD and microzooplankton grazing (MICRO GRAZ) rates (mg C m<sup>-2</sup>) based on flow cytometric populations *Prochlorococcus* (PRO), *Synechococcus* (SYN) and photosynthetic eukaryotes (EUK). b) PROD and MICRO GRAZ rates (mg C m<sup>-2</sup>) from dilution experiments based on Chla. MESO GRAZ based on the fraction of Chla removed by mesozooplankton d<sup>-1</sup> and integrated values of C:Chla. c) PROD and MICRO GRAZ of heterotrophic bacteria (HBAC).



**Fig. 12.** Relationships between euphotic-zone integrated estimates of phytoplankton production (PROD) and grazing (GRAZ) for phytoplankton and heterotrophic bacteria (HBAC) along the 110°E transect. a) Blue diamond (FCM) symbols are from combined flow cytometry populations (PRO, SYN and EUK) from Figure 11a; red circles (CHL) are Chla from Figure 11b, and GRAZ is combined micro- and mesozooplankton grazing (MICRO+MESO) from Figure 11a,b. b) HBAC PROD and MICRO GRAZ from Fig. 11c. All regressions are forced through zero.